UNIVERSITÀ DEGLI STUDI DI MILANO
FACOLTÀ DI SCIENZE MATEMATICHE,
FISICHE E NATURALI

Corso di Laurea in Fisica

Tesi di Laurea in Fisica Magistrale

OPTICAL SYSTEM FOR POSITRONIUM EXCITATION TO MEASURE GRAVITY ACCELERATION OF ANTIMATTER IN AEGIS EXPERIMENT

Relatore: Simone Cialdi

Correlatore: Fabrizio Castelli

Tesi di laurea di:

Giovanni Cerchiari

matricola: 790797

Anno Accademico: 2011/2012

Contents

Introduction

Antimatter is a symmetric status with respect to ordinary matter. Many quantities of antimatter particles, like charge, are opposite while others, like mass are equal. Among the symmetry tests between matter and antimatter the measurement of the gravitational interaction is missing. The Antimatter Experiment: Gravity, Interferometry and Spectroscopy (AEGIS) is an experiment at CERN whose primary scientific goal is the measurement of the Earth's local gravitational acceleration on antihydrogen. In fact behavior of antimatter in a gravitational field has not been tested yet and this measure could answer important questions about fundamental topics of the universe.

The first step to reach this goal is the production of antihydrogen. In AEGIS this antiatoms are obtained with a charge exchange reaction between antiproton and Positronium. Positronium is a bound state composed by one electron and one positron, thus forming a two charged body system like hydrogen. To enhance the synthesis cross section Positronium atoms should be excited to high energy levels. For this reason a laser apparatus has been developed at *Università degli Studi di Milano* in the laboratories of the physics department by Simone Cialdi, Fabrizio Castelli, Marco Giammarchi, Fabio Villa and with important contribution of all the students that joined this project for their graduate and master thesis. The excitation process is realized in two-step. In the first, corresponding to an ultraviolet radiation, Positronium is brought from ground to n = 3 state, and in the second, stimulated by infrared light, Positronium is subsequently excited to Rydberg levels.

Thesis' work has been focused on the finalization and installation of this laser apparatus at CERN. In particular during the thesis we followed development and installation of the optical system that transfer light radiations to Positronium excitation region.

The description of AEGIS apparatus follows from the experience acquired during the permanence at CERN for the installation of the optical system in November 2012. Positronium production process is discussed starting from the theoretical and experimental results accomplished by the physics department of *Università di Trento*. Their conclusions are recollected in a simplified model to describe the temporal evolution of the generated Positronium. This model has been used in the development of the optical system that guides laser radiation into Positronium excitation region.

The optical system realized for the thesis that connect the laser apparatus to AEGIS is described in details. Two different solutions are presented, one to transfer the infrared pulse and one for the ultraviolet radiation. Infrared is guided by an optical fiber, while ultraviolet reaches the excitation region via successive reflections. We studied the possibility to adopt an optical fiber to transfer the ultraviolet pulse. However, after the evaluation with experiment, this solution has been found not suitable for AEGIS, since the transferred power was insufficient. Thus the ultraviolet now gets to the excitation region in free propagation, guided by three prisms used in total reflection.

AEGIS Experiment

Introduction

Modern theories explain the interactions among bodies we observe in experiments as the consequence of four fundamental forces. These interactions are called electromagnetical, weak, strong and gravitational forces. The first three forces are order of magnitudes much stronger than gravity at particle levels, and by now we are able to measure gravity effects only on macroscopic scale, starting from the asteroids or cosmological dust and ending to the black holes. At the state of art of our knowledge on collider physics and accelerators the effect of gravitational force is negligible and useless to calculate cross sections and decay rates. These quantities can be deduced relaying only on the other interactions and thus gravity is nowadays kept aside in experimental particle physics. Studies on fundamental constituents of matter are grown as a consequence of interaction between technology and theory, driving theories in explaining the behavior of the universe well below the atomic scale. This fact has lead the physicists towards the quantization of fields as a solid basis for consistent theories of physical phenomena, and the previsions of these theories are at times in an astonishing agreement with laboratory tests. However in this picture gravity has played a second role, remaining outside the laboratories and relaying only on cosmological observation.

Theoretical physicists are nowadays concerned in quantizing General Relativity forward a unified theory of the fundamental forces. The best candidate for a “Theory of Everything” we have now is the Standard Model, a renormalizable quantum field theory based on gauge symmetries. In this framework the gravity should be explained as a new quantum field, leading to a force mediated by the exchange of particles. This point of view necessarily constitutes a departure from Einstein’s General Relativity and leads to important physical consequences that should be tested experimentally. The boson mediator of this force is called “graviton” and should be a particle of spin 2 (tensor particle). In addition to this tensor part, gravity could have scalar (spin-0) and vector (spin-1) components. While the tensor and the scalar part would lead to an attractive potential, the exchange of an odd-spin particle would have the opposite effect. Hence, the quantization of the theory brings out the possibility of both attractive and repulsive effect because of the different type of exchanged particles [1].

For this reason the investigation of the gravitational effect on antimatter could reveal new and unexpected effects, showing us new properties about the fundamental constituents of the universe. In fact the measure of a repulsive force would constitute an evident violation of the weak equivalence principle. This principle is a postulate of General Relativity that states the equality between the inertial and the gravitational mass. Over a century of experiment in the field of particle physics has established that the inertial masses of antiparticles are equal to their ordinary counterpart as we can deduce from CPT invariance of the actual theory. On the other hand no experiment until now has tested the gravitational interaction between matter

and antiparticles, thus leaving open many questions about this fundamental force. It should be stressed that there are a number of arguments against “anti-gravity” effects, i.e. a gravitational force with opposite sign. The most intuitive is perhaps Morrison’s argument [2], which demonstrates that such a phenomenon would violate conservation of energy, but it is not the only one. We can put some bounds to this hypothetical antigravity effect also from changes in cyclotron frequency of antiproton or from loop corrections with virtual particle in ordinary matter interactions [3].

Consequently, questions about the weight of antimatter deserve answers either to confirm or to suggest a serious rethinking of current theories. As a matter of fact two attempts has been made to reach this goal by experimenting over charged elementary particles at Stanford and CERN international laboratories (in particular at the Low-Energy Antiproton Ring), but no result has been achieved due to strong effects of the electric and magnetic fields used to confine these particles. AEGIS collaboration (Antimatter Experiment: Gravity, Interferometry and Spectroscopy) is trying to reach this goal using antihydrogen to dump down these unwanted secondary effects. Indeed antihydrogen is a neutral atom thus possessing a weak coupling with quasi static electromagnetic fields.

AEGIS experiment aims to obtain cold antihydrogen combining together the fundamental constituents: antiprotons and antielectrons (positrons). Antiprotons are provided by the Antiproton Decelerator, a facility at CERN dedicated to this task; while positrons are produced and controlled within the apparatus of the experiment. Once AEGIS will have neutral antimatter the gravity experiment will take place. A beam of antihydrogen will be accelerated horizontally and sent toward a Moirè interferometer to measure the typical trajectory of this particle under free propagating in the gravitational field of Earth. From the kinematic reconstruction of the motion it will be possible to measure the acceleration that antihydrogen perceives in a gravitational field.

The Antiproton Decelerator

The biggest limiting factor in the large scale production of antimatter is the availability of antiprotons. Antiprotons have a mass of about 1 GeV thus requiring big particle accelerators to reach the activation energy for pairs production.

The Antiproton Decelerator is a facility at CERN to produce cold antiproton to be used in experiments with antimatter. The AD was built as a successor to the Low Energy Antiproton Ring (LEAR) and started operation in the year 2000.

To provide cold antiprotons suitable for experiments, proton beams are fired by the Proton Synchroton (PS) accelerator towards a Be target. The collision energy is enough to create new proton-antiproton pairs that exit from target at almost the speed of light. After the target a mass spectrometer selects antiprotons among the reaction products injecting them into the deceleration ring. There a series of focusing and bending magnets keep antiprotons on the same track, while a few radiofrequency stages act for deceleration bringing the speed of antiprotons to 10% of the speed of light. After one minute production and deceleration

processes have come to end and a bunch of about 10^7 antiprotons having an energy of 5 MeV is ready to be delivered to the experiments.

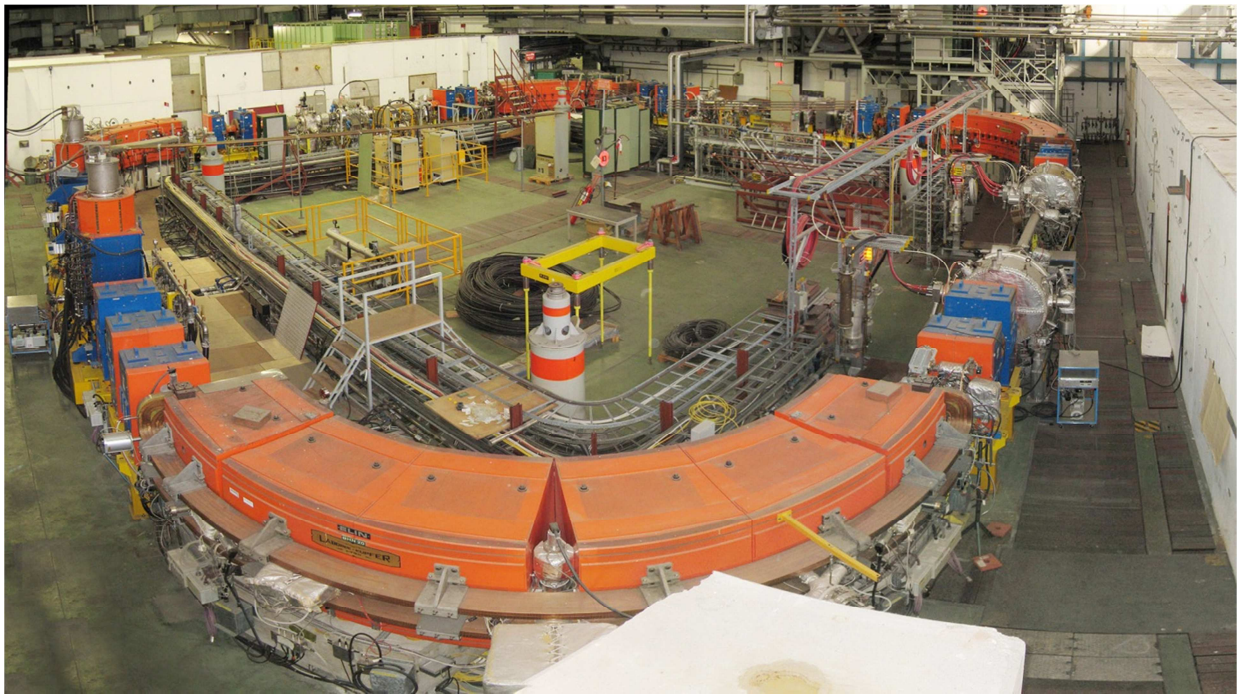

Figure 1 – A picture of the Low Energy Antiproton Ring the prototype experiment of the Antiproton Decelerator.

AEGIS experimental zone

In addition to AEGIS other experiments are currently working with antimatter. ALPHA and ATRAP are working to trap antihydrogen to prevent the annihilation by ordinary matter and ASACUSA is studying mixed systems of matter and antimatter. AEGIS experiment, like the others, is installed inside the ring of the Antiproton Decelerator aligned to the assigned beam line.

In particular, in AEGIS beam line of antiprotons is collected by a 5T magnet where the antiprotons are trapped and cooled down. After this process the antinuclei are pushed in the second magnet in the so called “central region” where the production of neutral antimatter is foreseen to take place. Positrons, the second fundamental ingredients of antihydrogen, are produced by radioactive decay of a sample of ^{22}Na and trapped in a Surko trap over the antiproton beam line. Finally, they are guided into the central region passing through the 5T magnet in the same trap that is used to capture antiprotons.

On one side of the 5T magnet an optical table is placed. Here a laser system generates pulsed radiation at suitable frequencies, which are used in the complex process of antihydrogen synthesis, as explained in detail later.

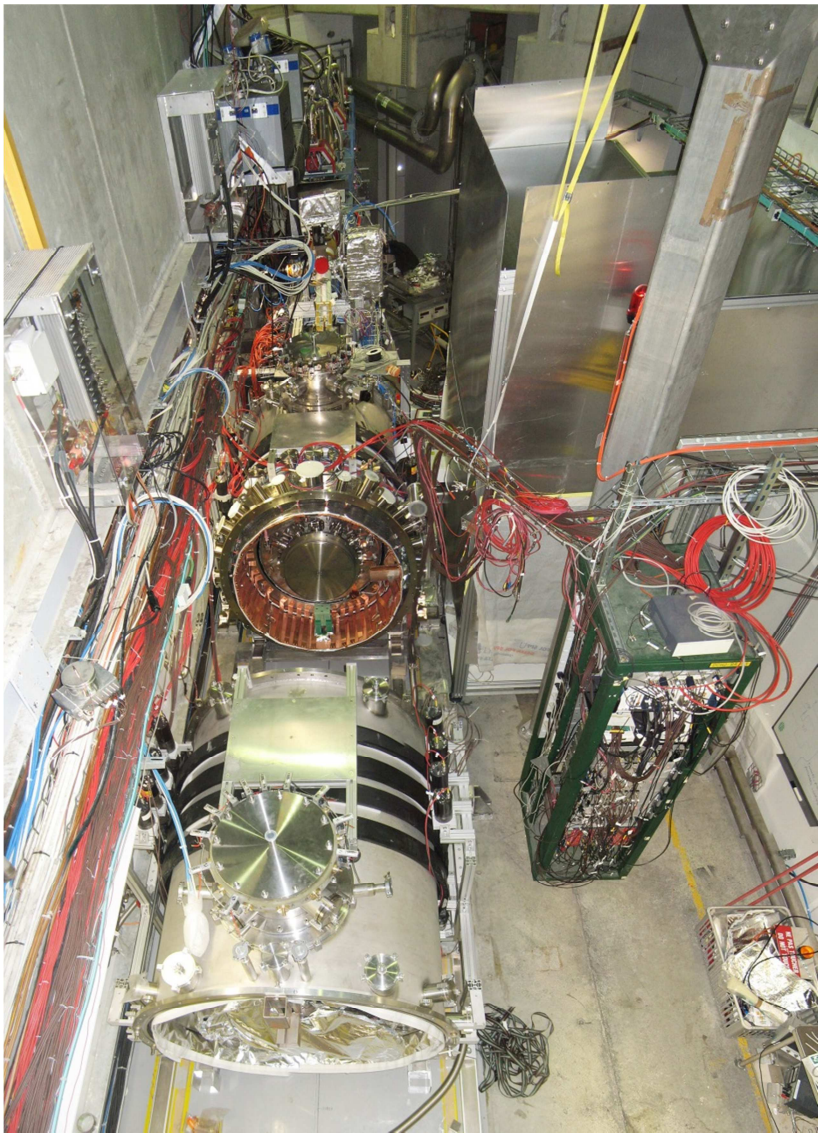

Figure 2 – AEGIS experimental zone a few days before the final assembly of November 2012. In foreground separated from the rest of the experiment is the "1T magnet" apparatus, following in the background the "5T magnet" is visible. On the right of the 5T magnet the laser table is located enclosed among aluminum shields

Antiproton trapping and cooling

To measure the antihydrogen interaction with the Earth gravitational field AEGIS needs first to obtain the raw materials and build up neutral antimatter. Inside the experiment a large section of the set-up is dedicated to the production of antihydrogen, starting from cooling and bunching of antiprotons and positrons, and reaching the final recombination of the two constituents. Mass of antiprotons is much greater than that of positrons, thus constraining the recombination temperature of the synthesized antihydrogen to be almost the same of the bare nuclei. It is important to stress that the measurement of gravitational interaction is of course affected by uncontrolled momentum distribution of produced antimatter. For this reason it should appear quite natural that AEGIS has dedicated part of the experiment to cool down and

trap antiprotons. Producing low momentum antimatter is the first requirements to perform the ballistic measurement.

Antiprotons' trapping is performed by a cylindrical superconducting magnet of 5T field. The cylinder axis is oriented towards the beam line coming from AD. In this way charged antiprotons injected by the decelerator are radially confined due to the effect of the strong magnetic field. To perform trapping and cooling procedures a number of cylindrical electrodes is displaced along the axis of the magnet. Electric potentials on electrodes can be regulated at will within few kV in order to confine charged particles in the axial direction, thus concluding the structure of a Penning trap. As recently tested this part of the apparatus enables AEGIS to trap a bunch of almost 10^5 antiprotons each AD injection.

Once AD is ready to send a bunch of antiprotons, a titanium foil is mechanically placed at the entrance of the magnet as degrader and, on the opposite side of the trap, the last electrode is driven to a suitable high potential. Antiprotons are in this way moderated by the degrader and axially reflected back by the action of the electrode. Trapping is realized suddenly turning on the potential of the first electrode, near the degrader, when the bunch of antiprotons is inside the magnet. Antiprotons are in this way confined along magnet length. They need to be cooled and compressed before entering in the following experimental zone.

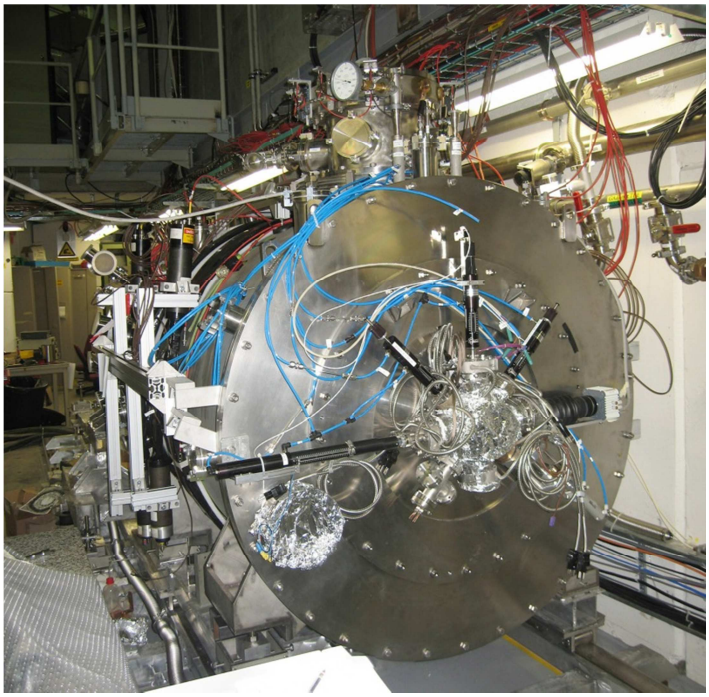

Figure 3 – Front picture of the "5T magnet" experimental section. Pneumatic actuators are displaced radially around the axis of the magnet to insert different experimental tools along the beam line.

Inside the magnet a tungsten cathode releases electron by thermionic effect. Electrons and antiprotons have the same charge and repeal each other by Coulomb interaction. In this way antimatter is prevented from annihilating with matter, while heavy nuclei can cool down transferring momentum to lighter electrons. Once this stochastic cooling has brought the

antiprotons to the desired temperature of a few electronvolts, the bunch of antiprotons is axially compressed and sent to the next stage of the experiment.

At the end of the 5 T magnet the beam line continues enters the “central region” where the antihydrogen production is foreseen to take place.

Antihydrogen production and gravity measurement

In the last twenty years Anti-Hydrogen has been produced in several experiments at CERN like ATHENA and ATRAP. The experimental observation of antimatter in bound state has proven the possibility of forming neutral antimatter particle aggregates. As reported by ATHENA collaboration antihydrogen annihilates isotropically on trap walls; while antiprotons, that are charged, break up this symmetry being influenced by any slight field fluctuation [4]. In those experiments this feature was used to identify antimatter annihilation, combining the position measurement with the spectra of the gamma rays emitted. In AEGIS the isotropic behavior of antihydrogen is particularly appreciated because it is necessary to get rid of any systematical error in trajectory reconstruction. With bare antiprotons in fact force fluctuations due to external and uncontrolled electromagnetic fields would overtake gravity effect. This is the main reason to try to perform the experiment using neutral antimatter, and so the need of producing cold antihydrogen.

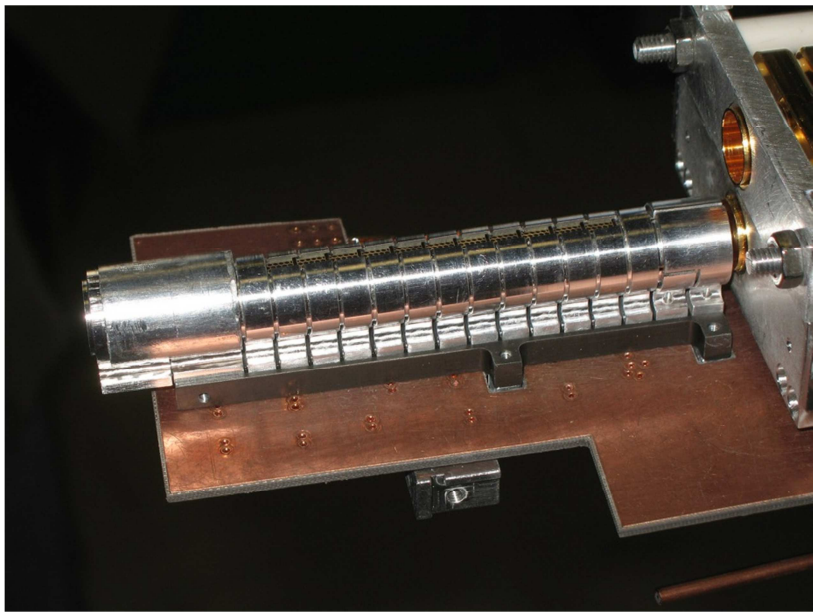

Figure 4 – Antihydrogen Trap – In this trap antiprotons are stored waiting for Positronium. Ps atoms are produced above this trap and reach the antinuclei through the thin holes that are visible in the upper part of the electrodes

The simplest experimental scheme that is possible to design for obtaining antihydrogen is the one adopted in ATHENA. In that experiment, antiprotons and positrons were mixed

together waiting for the recombination to happen. In this way antihydrogen was produced for spontaneous radiative recombination (SRR) between positrons and antiprotons:

$$e^+ + \bar{p} \rightarrow \bar{H}^* + \gamma$$

where the apex star symbol indicates that antihydrogen is produced in an excited state. This is the time-reversed process of photo-ionization and appears a slow process on the typical time scales of collisions among atoms and ions in the Penning trap. The cross section depends only on the kinetic energy $E_{\bar{e}}$ of the antielectron in the center of mass frame of the antiproton and the capture level m. The partial cross section decreases for high m; while the total cross section is obtained summing all the contributes of each m level up to a "cut off", corresponding to the bound state which can be ionized by collisions. Typical values of the cross section range from $5 \cdot 10^{-21}$ to $1.5 \cdot 10^{-16}$ cm^2 and can be enhanced by a factor of 80 by using suitable radiation to stimulate the emission of a photon, thus lowering the energy of the atom [5].

In AEGIS antihydrogen is foreseen to be produced with a charge exchange reaction between antiprotons and Rydberg Positronium (Ps). Positronium is an unstable bound state composed by a positron and an electron. Before the combination with antiprotons Positronium needs to be synthetized and excited. Thus the proposed method is remarkably different and more complicated, but expected more efficient than the others adopted in the past and by other experiments. Properties and production apparatus of Ps is discussed in a different chapter. Now we will consider only the charge exchange reaction, which have already been demonstrated successfully by ATRAP collaboration:

$$Ps^* + \bar{p} \rightarrow \bar{H}^* + e^-$$

The main reasons that make this reaction interesting for AEGIS design are the following. First the reaction has a large cross section which is of the order $a_0 n^4$, where $a_0 = 0.05$ nm is the Bohr radius and n is the principal quantum number of the Ps. Furthermore antihydrogen is produced in Rydberg excited levels with a predictable state population strictly related to that of the incoming Positronium. The range of final quantum states turns out to be reasonably narrow. Thanks to the sensitivity of these Rydberg states to electric field gradients, an antihydrogen beam can be formed by accelerating atoms with a time dependent inhomogeneous electric field. Another important reason to prefer the exchange scheme is due to the possibility of experimentally implement the reaction in such a way that very cold antihydrogen can be produced. To maximize the efficiency and the quality of antihydrogen beam is surely important for the gravity measure and its transverse velocities should be kept as low as possible.

A Monte Carlo [31] simulation has been implemented in order to understand the formation process under the experimental conditions of AEGIS, and to optimize production rate of useful antihydrogen atoms. A few results of this simulation are reported in the figures of this paragraph.

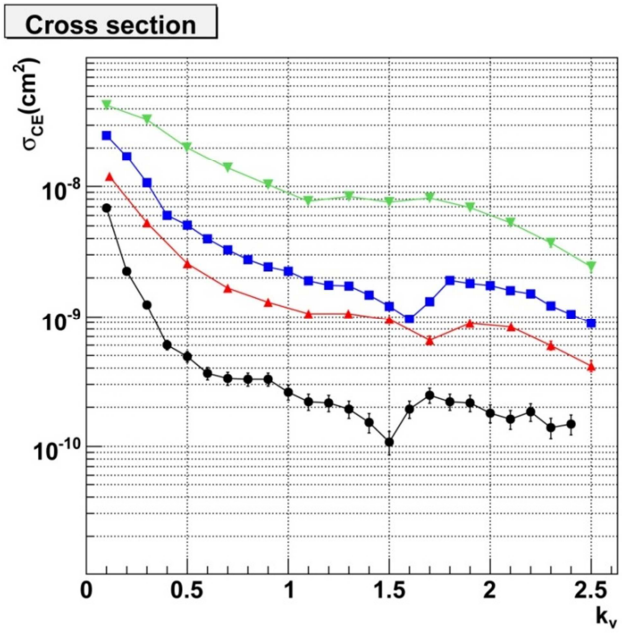

Figure 5 – In this plot is shown the cross section of the exchange reaction is shown for different value of the principal quantum number of Positronium. From top to bottom n = 50, 35, 30, 20 while l=2 for all the lines. k_v is the ratio between the translational speed of Positronium over its averaged speed for circular orbits. The corresponding velocities for k_v = 1 are 22 km/s, 31km/s, 36 km/s, 54km/s

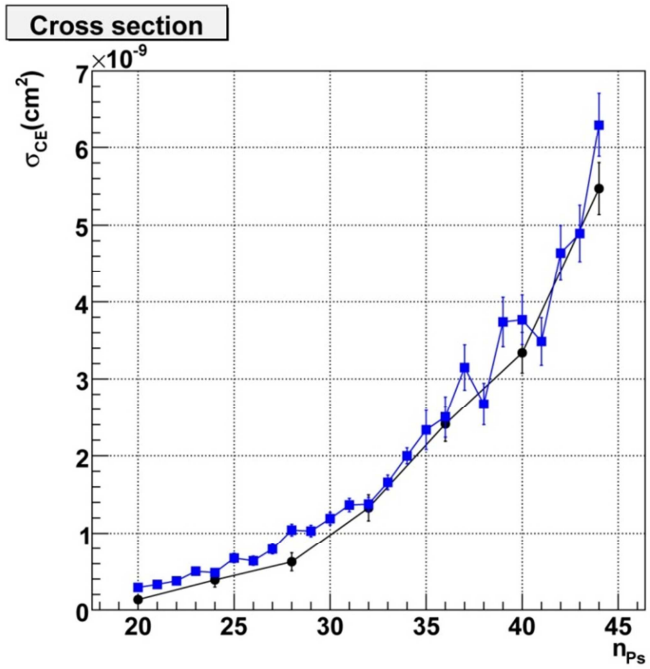

Figure 6 – The plot show the cross section for antihydrogen formation versus the Positronium principal quantum number n_{Ps}. In this simulation Ps has been initialized fixing the ratio between the translational speed of Positronium over its averaged speed for circular orbits to unitary value. In this way it is possible to appreciate that the cross section is depending on the average speed of the e+ e- components rather than on the orbital quantum number l. Squares refer to orbital quantum number l randomly chosen between 0 and n_{Ps} − 1 while circles correspond to l = 2

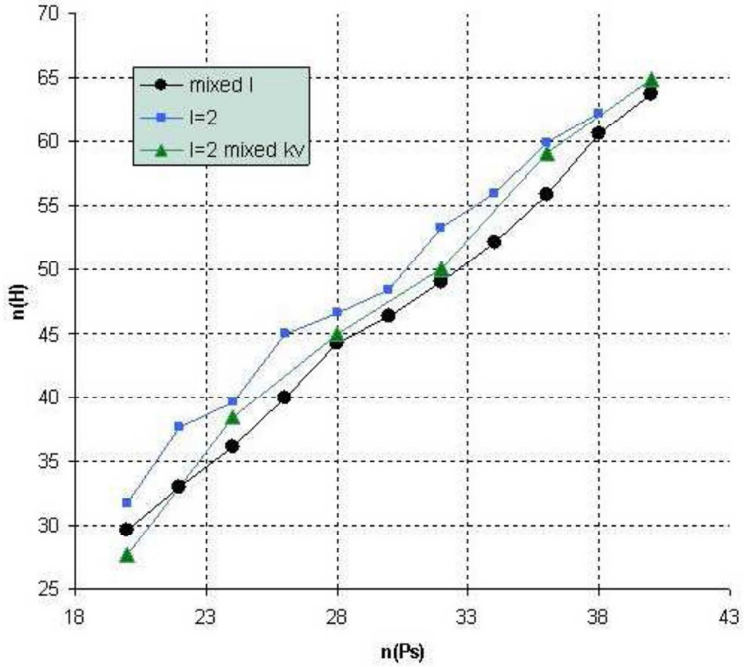

Figure 7 – This plot show the mean value of the principal quantum number of the produced antihydrogen n(H) versus the principal quantum number of Positronium n(Ps). Square refers to orbital quantum number of Positronium fixed at value l = 2 and k_v = 1 . k_v is the ratio between the translational speed of Positronium over its averaged speed for circular orbits. Circles and triangles refer to similar condition in which respectively l and k_v are randomly chosen.

Once antihydrogen is produced it has to be guided out of the trap by coupling its dipole moment with an electric field gradient, thus obtaining a few atoms of antihydrogen in free propagation outside the trap in the horizontal direction. At this stage the trajectory of antimatter will be reconstructed by the Moiré deflectometer placed after the trap, at the end of the experimental apparatus.

The deflectometer consists in two identical gratings and a silica detector, placed at equal distances L from each other. They are mounted transversally to the beam propagation direction. These gratings prevent some antihydrogen from propagating further, thus producing an annihilation pattern at the location of the detector similar to an interference pattern. That pattern has the same period d as the gratings and with particles in free propagation the fringes should be aligned to the aperture of the gratings. On the contrary under the influence of a transverse acceleration g field they should be vertically displaced (particles ‘‘falls”) by a distance δx depending on their initial velocity v:

$$\delta x = -g\left(\frac{v}{L}\right)^2$$

In common devices the experiment is performed with three gratings. As an example a three-grating Moiré deflectometer has been used to measure the local gravitational

acceleration to a relative precision of 2 10^{-4} with a beam of argon atoms traveling at an average velocity of 750 m s^{-1}. In this type of experiments the third grating is in place of AEGIS' detector and act actively introducing a selective path along the beam line. In AEGIS experiment, thanks to the particular nature of the object under analysis a position sensitive silica annihilation detector is adopted instead of the third grating. This improvement is required by the scarce number of antihydrogen and is foreseen to increase the overall transmission of the apparatus by the inverse of grid's open fraction (roughly a factor of three).

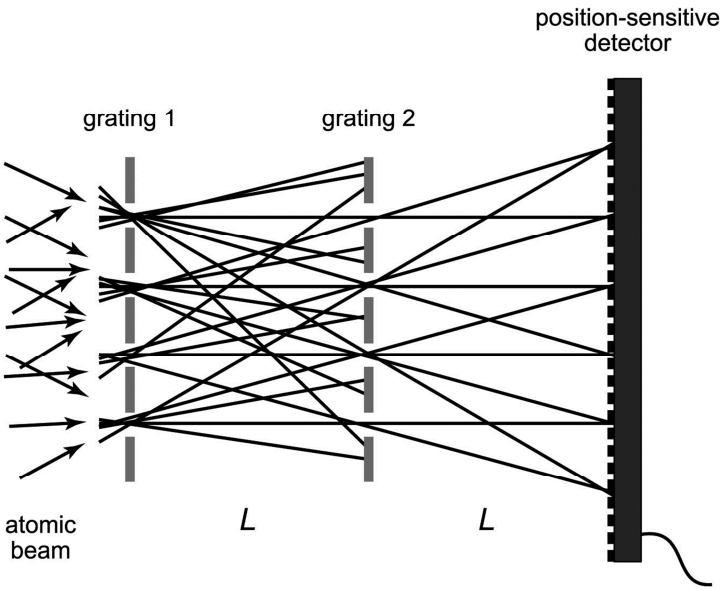

Figure 8 - Principle sketch of the Moire´ deflectometry technique with two identical gratings and a position-sensitive detector

Such a device does not necessitate trapped atoms and is very suitable with antimatter detection. Obtaining cold antihydrogen is particularly desirable in order to reduce the uncertainties in gravity measurement. The ballistic trajectory estimation is affected by the average random velocity of the antihydrogen that for this reason should be reduced as much as possible. To achieve cooling of the antiatoms it is possible to manipulate antiprotons before recombination, thus reducing the transverse dispersion of the speed of antihydrogen to minimum levels acting on the charged components. The nucleus is the massive part of any atom, thus cooling antiprotons leads as consequence an overall cooling of the final antimatter cloud. To enhance the measurement performance a technique of indirect stochastic laser cooling of antiprotons is under study [6]. The cooling should be achieved by mixing with heavy negative ions opportunely precooled anions. In recent years a few atoms belongings to the family of lanthanide (like Os or La) have been discovered to have a suitable energy transition to be laser cooled as anions. Antiprotons mixed in the same trap with cooled La^- should transfer their momentum to these atoms ending up with a lower average kinetic energy.

Figure 9 – In picture trap system of the "central region" of the experiment. Trap is mechanically supported by the inner flange that separates Ultra High Vacuum region (10^{-10} mbar at 4K) with intermediate region (10^{-7} mbar at 70 K)

Positronium

The simplest scheme to produce neutral antiatoms is to mix in the same place antiprotons and positrons and wait for antihydrogen atoms coming out. Of course, previous experiments before ATRAP and AEGIS had already obtained cold antihydrogen in this way. These techniques usually adopt a linear Penning trap divided in two sections, one dedicated to antiprotons and the other dedicated to positrons. When both components are ready, antielectrons are pushed onto the antinuclei cloud. This is the most obvious scheme in which all the fundamental building block of antimatter are produced separately and then mixed together without other treatments.

In AEGIS the combination of antiproton and positrons to obtain cold antihydogen is going to be realized in a more efficient way by mixing antiprotons with high excited Positronium atoms (Ps) inducing a charge exchange reaction. Positronium is an unstable bounded state composed by an electron and a positron. The decision to include a further step and to adopt Ps is due to higher cross section of the charge exchange reaction with respect to recombination with bare positrons. This technique could in principle increase of some order of magnitude the number of antiatoms produced as a consequence of the greater cross section. On the other hand, this solution is paid with a more complicated apparatus where in addition to positrons trapping, Ps must be produced and excited to Rydberg levels (states with high principal quantum number) before the interaction with antiprotons.

The current apparatus is designed to implant positrons in a special target made by silicon, waiting for a cloud of Positronium to emerge backscattered from the silica surface (oxidized silicon). Note that Ps is a neutral atom thus difficult to be controlled by electromagnetic fields. For this reason excited Positronium has to be created close to the final antiprotons trap leaving free Ps to spread inside the experiment. This type of set up has the consequence of splitting in two sections the experimental apparatus dedicated at Ps. The first part is aimed to bunch positrons from a radioactive source of ^{22}Na and the second, near final antiproton trap, to produce and excite Ps. Excitation toward Rydberg states is performed by the laser system built in Milan which will be described in a following chapter; in this section we will discuss the experimental set up to produce Ps from positrons.

Positronium atom

Positronium (Ps) is an unstable atom consisting of an electron and a positron. The two particles tend to annihilate each other with characteristic lifetimes, producing gamma ray photons. The set of atomic energy levels of Ps is, in a certain sense, similar to that of the hydrogen atom because both are two charged particle systems governed by the same dynamical equations. However the masses of the positive charged constituents are not the same leading to different lines in the spectrum.

Like Hydrogen the energy levels in Coulomb approximation are a function of the principal quantum number n only. Energy E_n is expressed as a function of elementary charge of the electron q_e, Planck's constant h, vacuum electrical permittivity ϵ_0 and reduced mass of the two-body system $\mu = \frac{m_1 m_2}{m_1 + m_2}$:

$$E_n = -\mu \frac{q_e^4}{8h^2\epsilon_0^2} \frac{1}{n^2} \quad (1)$$

For each n energy level, in Hydrogen a sublevels structure can be observed, due to small energy corrections from hyperfine and eventually magnetic (Zeeman) interactions.

Energy levels of Positronium have been studied to the aim of exciting the atom to Rydberg levels by laser pulses, to favor antihydrogen production. The main difference between the Hydrogen atom and Ps resides in the reduced mass. Calling m_e the mass of the electron for Hydrogen we obtain $\mu \cong m_e$ while for Positronium $\mu = \frac{m_e}{2}$. Thus at first order the ratio of the corresponding energy levels is separated by factor of two.

The energy levels formula above reported is calculated for the two-body system in isolated environments, but the experimental conditions of AEGIS are far from isolated, due to a 1T magnetic field in the region where Ps should be produced, excited and mixed with antiprotons. Here a big difference with respect to the Hydrogen atom can be observed. Due to the very low mass of the system, and consequently very high velocity, the greater correction to the energy levels for high n is due to the Motional Stark effect, whose contribute is overwhelming with respect to other energy level correction coming from hypherfine and Zeeman interactions. In the Motional Stark effect, a charged particle that is moving with respect to a magnetic field will perceive an electric field in its own frame of reference. Since all physical quantities of interest are usually evaluated with atoms at rest, this electric field should be included into the model for Ps energy levels. The electric field couples with the electric dipole operator of the system splitting energy levels with different angular momentum. As a consequence, in the magnetic field of the experimental region, a complete mixing of energy sublevels is realized for n > 15, as shown in Figure 10. In that region the unperturbed quantum numbers lose their significance and optical transition are not subject to dipole selection rules. This is of paramount importance for planning and realization of a suitable laser system for excitation.

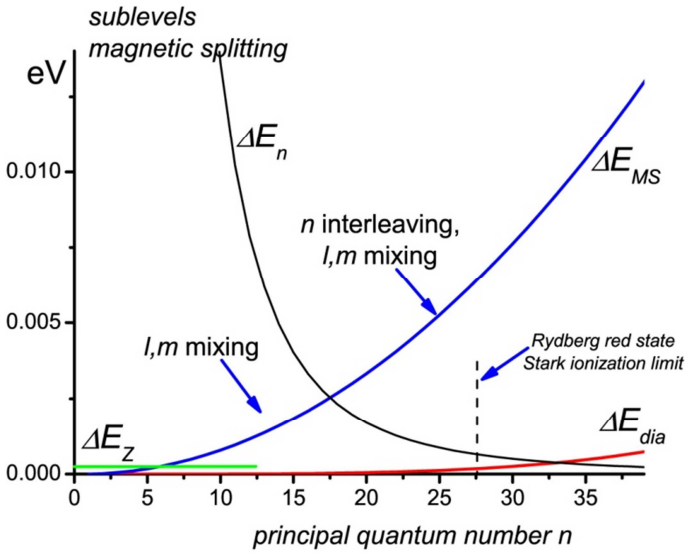

Figure 10 – Contributes to the energy sublevel splitting of Ps with respect to principal quantum number. ΔE_n is the difference between bare energy levels determined by principal quantum number (see eq. (1)), ΔE_{MS} stands for the motional Stark effect, ΔE_Z and ΔE_{dia} account for the Zeeman and diamagnetic contributions

Ground states of Ps are particularly important since they are the dominant channels of production. There are two possible configurations, depending on relative orientations of the spins of electron and positron. The state with antiparallel spins (singlet state) is known as parapositronium. It has a mean lifetime of 125 picoseconds and decays preferentially into two gamma quanta with energy of 511 keV each. The state with parallel spins (triplet state) is called orthopositronium and is three fold degenerate in absence of magnetic fields. The triplet state has a mean lifetime of 142 ns and the leading mode of decay is in three gamma photons.

Parapositronium has formation probability of 1/4, while orthopositronium has formation probability 3/4. The excited states are not naturally produced and are commonly obtained exciting the atom by laser radiation. In AEGIS, Ps excited to Rydberg levels are used for antihydrogen production because these states are scarcely bounded and the split up of the atom is favored during the charge exchange reaction. Due to the relatively large distance between particles, excited Ps has longer lifetimes: first Ps has to decay radiatively to the ground state and then it annihilates. It happens that for Rydberg states the radiative decay rate is order of magnitudes lower than the annihilation time, therefore we shall assume that the lifetime of the atom is equal to the radiative lifetime of the excited state. An upper bound formula for this time (precise at 10%) has been found in the middle ’80 [12] and is an explicit function of the principal quantum number n and the orbital quantum number l:

$$\tau_{nl} \sim (1.87 \cdot 10^{-10}\ s)\ n^3 \left(l + \frac{1}{2}\right)^2$$

From this expression we learn that states with high angular momentum have longer lifetimes and lifetimes of Ps can be estimated with a n^5 proportionality factor.

Apparatus

Positrons are created in the decay line of ^{22}Na. They exit randomly distributed from the radioactive medium, but still too energetic for the purpose of the experiment. For this reason a thin parabolic surface of frozen Ne is placed in front of the Na salt, to moderate and to guide positrons towards the beam line under a sufficient solid angle. After this stage a remarkable part of the apparatus is dedicated to convert the continuous flow of positrons from ^{22}Na into compressed packets. In order to obtain a bunch, positrons are trapped and stored in two similar Penning traps. The first is more oriented to trap antielectrons while the second is dedicated to accumulation. The working procedure of these two stages is quite similar to the trapping scheme of antiprotons into the 5T magnet; however in this case the stochastic cooling is achieved using ionized noble gases instead of electrons.

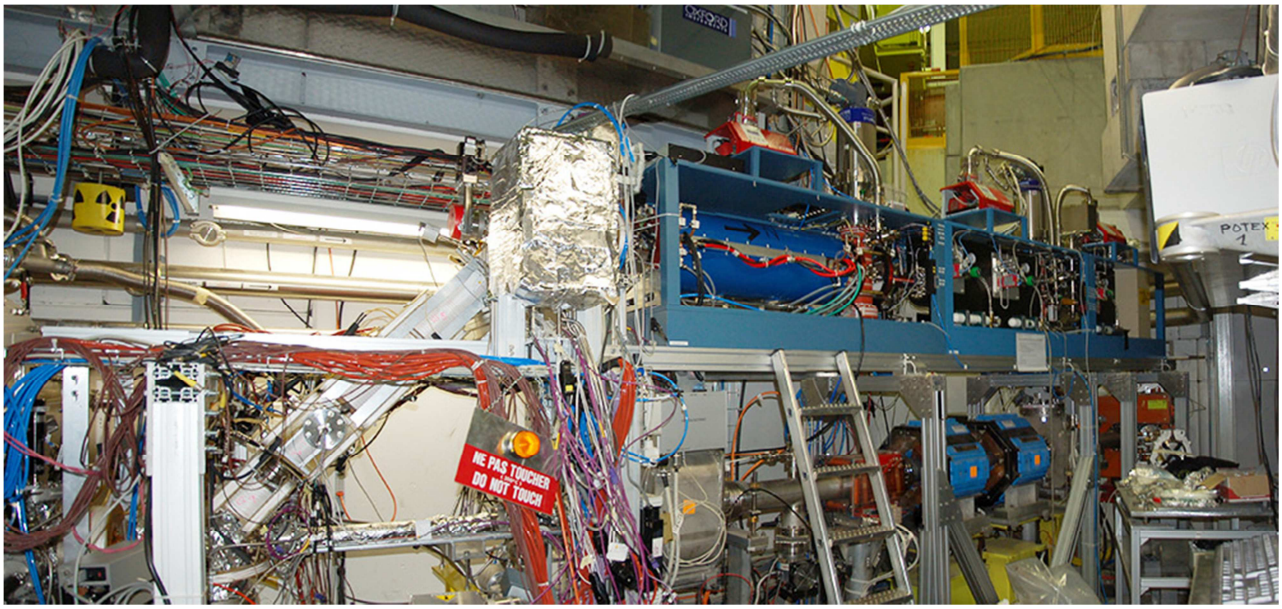

Figure 11 – This picture shows the positrons apparatus placed the antiprotons beamline coming from AD. Positrons' apparatus is divided in three different stages by blue boxes. From right to left there is the ^{22}Na source with the Ne moderator, the trap and the accumulator. After the accumulator, the transfer line on the left guides the positrons towards the 5T magnet.

This section of the apparatus, from production to bunching of positrons, is placed over the antiproton beam line coming from the AD. In particular the two lines join before the entrance of the 5T magnet. Once the number of positrons is about 10^5-10^6 the accumulator is ready to push the antielectrons into the transfer line when requested by the experiment. Bunching of positrons has twofold benefits. From one side it is necessary to produce as much antihydrogen as possible in a short while because in AEGIS there are no traps for neutral particles; in fact the experimental scheme is first to produce as much antihydrogen as possible at once and then kick it towards the gravity measurement interferometer. Moreover it is possible to excite Ps using pulsed light. In fact it is much more convenient to excite a group of atoms in a single burst, rather than introducing a continuous flow of energy that heat up the system. Remember

that the experimental region where antihydrogen is going to be produced should be kept at 4 Kelvin degrees and so any unnecessary heat source should be avoided.

Positronium, as mentioned, needs to be synthetized in the central region of the experiment, near the final antiproton trap. Ps is neutral and after production is free of propagating in the experimental without being influenced (at last in first approximation) by all magnetic and electric fields generated by the magnet and the electrode of the traps. To maximize the probability that a Positronium reach an antiproton the target is placed over the trap to let Ps diffuse towards antiprotons on the whole length of the trap. However in this way the final positron trap should be vertically displaced with respect to the principal beam line where the antiproton trap is mounted. As a consequence target orientation should allow from one side to succeed in positron implantation and from the other to maximize Ps diffusion in the direction of antiprotons. The compromise solution adopted tilts the target at 30° with respect to the beam line.

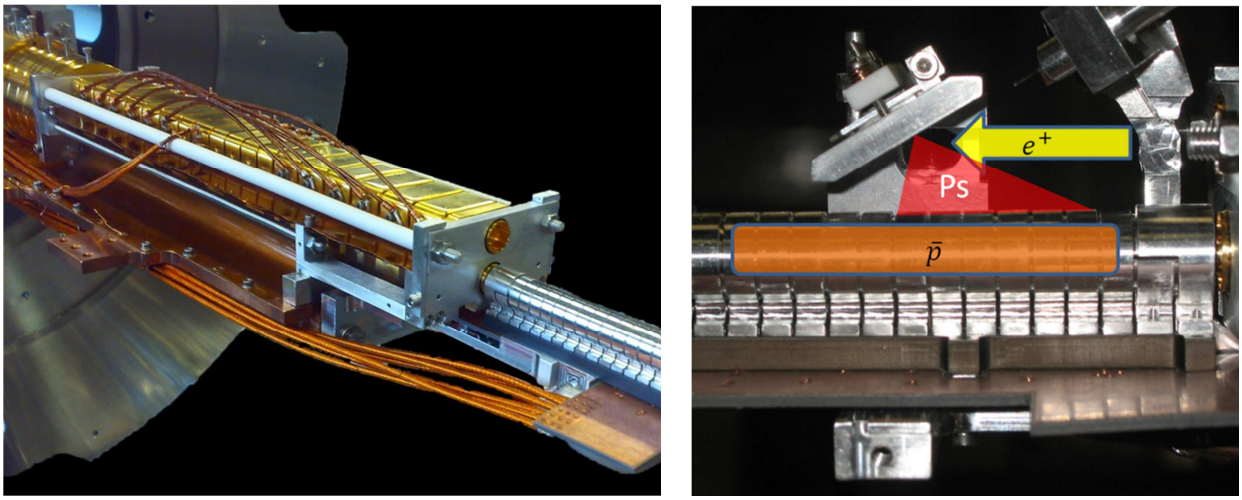

Figure 12 – In left picture the positrons trap is displaced over the antiproton beam line. This trap is used to implant positrons in the Si target. Orientation and position of the target with respect to antiprotons are shown in right picture. The angular behavior of Ps is drawn for a pictorial representation only.

Distribution of generated Positronium

The technique for Positronium production has been developed at the *Dipartimento di Fisica* of *Università di Trento* [13-15]. Here we report their experimental and theoretical results to propose a simplified model for the evolution of the generated Positronium.

To obtain Positronium atoms, positrons are accelerated toward a silicon target where holes of 5-8 nm of diameter by 2000 nm depth are dug. Average distance between holes is comparable to their diameters. These quite remarkable nanochannels perpendicular to the surface can be obtained by electrochemical etching of Si in hydrofluoric acid (HF) solution. After etching the target is exposed to fresh air in a temperature controlled environment so that the holes are oxidized in controlled condition to favor Positronium formation.

Positrons arriving on the target at 7 KeV (5 ns in duration) are implanted on average at 700 nm depth. In metals and semiconductors the formation of Ps in the bulk of the material is prevented by the high electron density and positrons undergoes a random walk of thermalization with typical diffusion length of about 200 nm. Actual models for the process suggest that positrons thermalize interacting with the phonons of the crystal. Due to the high diffusion length and to the closeness of nanochannels, the majority of positrons reach the silicon oxide interface. In these solids Ps formation is only a surface process: a thermalized positron diffused to the surface can capture an electron from SiO_2 and then be adiabatically emitted as Ps. The atom has now an average kinetic energy beetween one to three electronvolts, yet it is still inside the medium. Subsequently Ps atoms bounce on walls holes before exiting; consequently a considerable fraction is emitted at the same temperature of the target.

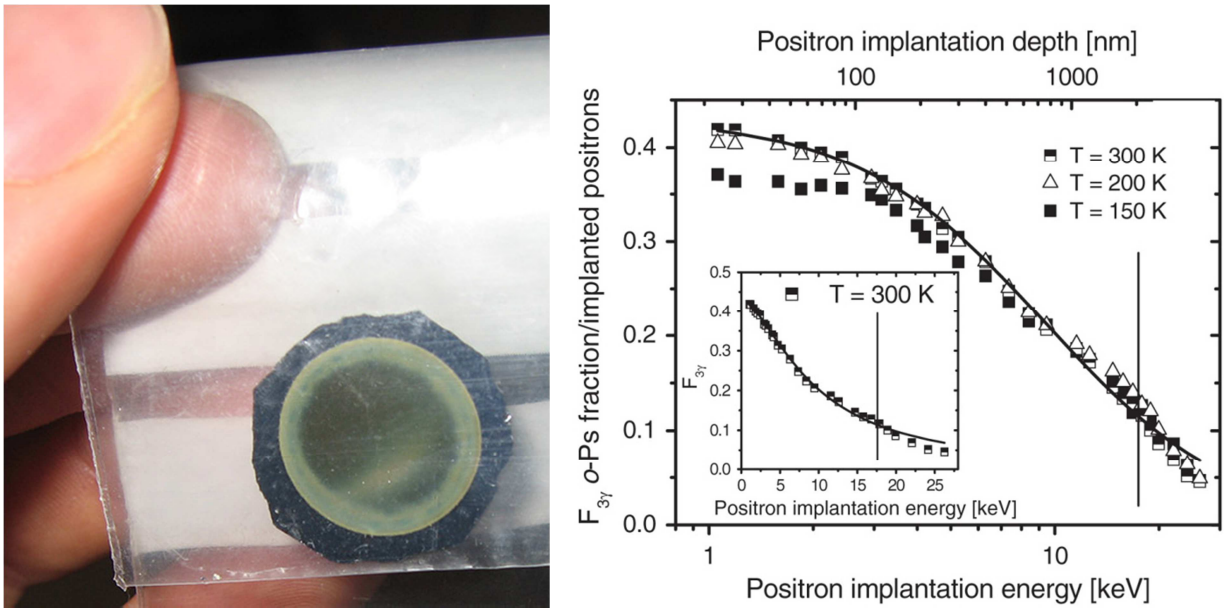

Figure 13 – In the picture is visible a sample of the Si target before the installation. The plot shows the orthopositronium fraction $F_{3\gamma}$ v.s. positron implantation energy (lowerscale) and mean positron implantation depth (upper scale). The continuous lines are best fits to the data. The vertical line marks the border between the Si layer with channels and the Si bulk. The RT curve in a linear scale is shown in the inset. The error bars are inside the symbols. Different temperatures correspond to different thermalization condition of the target.

This technique has been deeply studied for high Ps production obtaining a meaningful cooled fraction of Positronium below room temperature. Variation in oxidation grade, sizes and distances among channels has been optimized before the adoption in AEGIS. After implantation with the target held at 150 K about 27% of positrons produce positronium that escapes into vacuum. Around 9% of the escaped positronium is cooled by collisions with the walls of nanochannels and is emitted as a Maxwellian beam at 150 K. Exiting fraction of Ps was estimated with a time of flight measurement detecting the time between positron implantation in the target and orthopositronium annihilation in flight. These measurements show that the distribution spectrum of exiting Positronium can be modeled with two

Maxwellian distributions with different characteristic temperatures. First temperature is closed to the temperature of the target and the second one is one order of magnitude greater. Tuning of the nanochannel's size was found to be crucial in obtaining Positronium clouds in vacuum at very low temperature. Ultimate limit depends on quantum laws of Ps atom confinement in nanochannels that establish the minimum energy achievable by Positronium. For holes of 5 nm in diameter this limits correspond to a Ps temperature of 116 K, while for channels with 8 nm diameter the temperature can be lowered to 45 K.

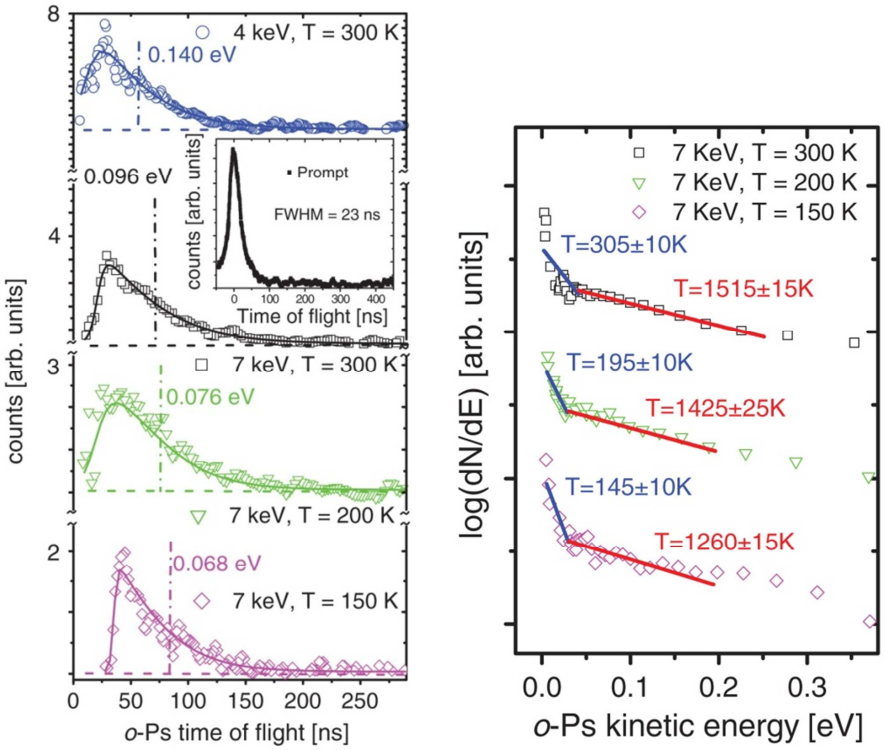

Figure 14 – Time of flight measurements and Maxwell distribution fits. T is the temperature of the Si target. The graph on the left shows the time of flight measurement of Positronium. The exiting fraction of Ps was estimated with a time of flight measurement detecting the time between positron implantation in Si and annihilation in flight. The gamma rays emitted by Positronium self-annihilation were detected with a NaI (Tl) scintillator placed behind an 11 cm thick tungsten shield, with a slit of 5 mm width. The center of the slit was located at 8.9 mm from the target surface which represents the flight path of Ps during its lifetime. The graph on the right show the energy distributions of exiting Positronium fitted with two Maxwellian curves.

Time of flight measurement of Positronium decay combined with the fits with a Maxwellian distribution can be used to estimate the size of the Ps cloud exiting from the Si target. Size of the generated cloud had to be taken into consideration for the development of the optical system for Positronium excitation. In order to obtain excitation laser pulses must hit at best the Positronium cloud. Indeed it is possible to figure out the superposition between the laser and the Positronium cloud as if the laser is taking a snapshot of the cloud with a 5 ns time exposure. The processes of light generation and Ps production must be synchronized and

both beam shapes and the delay should be adjusted to mask the possible experimental uncertainties in working conditions. Here is going to be discussed the typical behavior of the Positronium cloud leaving the problem of synchronization after the description of laser apparatus.

For our purposes we will try to reconstruct the experimental results of time of flight measurements by combining only one Maxwell distribution for Ps atoms speed with the decay laws of orthopositronium. After this calculation we will express this function v.s. the distance from the target, rather than with respect to time, to figure out how big is the Ps cloud when we take the "snapshot" with laser pulses.

The probability for a Positronium to exist after a time t is given by

$$P_\tau(t) = e^{-\frac{t}{\tau}}$$

where τ is the typical decay time of orthoPositronium and is equal to 142 ns.

The Maxwell distribution for speed is given by

$$p(v) = \left(\frac{m}{k_b T}\right)^{\frac{3}{2}} \sqrt{\frac{2}{\pi}} v^2 e^{-\frac{1}{k_b T}\frac{1}{2}mv^2}$$

Since we are in nonrelativistic limit we should expect no dependency of the decay rate on the motion of Ps. Thus probability that a particle with assigned speed v will still exists at time t is given by the product of two distributions:

$$P(v,t) = p(v)P_\tau(t)$$

Now we must consider that the time of flight measurement has been realized observing the Ps decay at 8.9 mm from the surface of the target. As a consequence we must express the probability density function $p(v)$ as a function of the distance x from the Si. Thus

$$P(v,t) \to P(x,t) = \frac{1}{t} p\left(\frac{x}{t}\right) P_\tau(t)$$

Notwithstanding the fact that we are completely disregarding the double trend in the speed distribution this function ends up to be a still acceptable approximation of the time of flight experiment; even when the typical temperature extracted from the fit of fast Positronium is substituted into the formula. For this reason we prefer using this simple approximation to estimate the size of the Positronium cloud exiting from the target for a given temperature distribution. As a matter of fact we are interest in the worst case scenario in which Ps is exiting really fast from the target compressing all the available timings. By now it is not yet well understood if it will be more convenient to produce antihydrogen with fast or slow Positronium. As a consequence we will evaluate all the typical physical quantities in worst case approximation using fast Positronium only, with typical temperature of $T =$ 1000-1500 K.

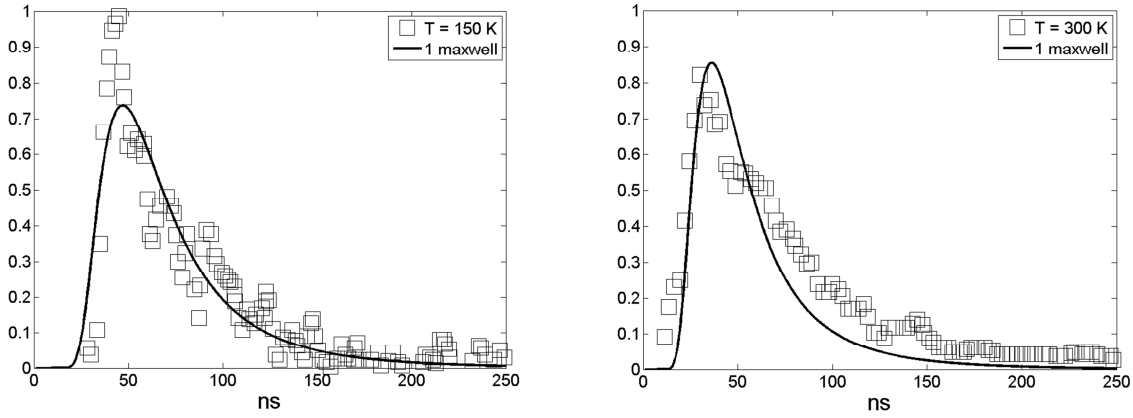

Figure 15 – Time of flight measurement with single Maxwellian speed distribution fit. The temperature is estimated to be (1.4 ± 0.4) 10^3 K when the target is held at 150 K while (2 ± 1) 10^3 K when the target is held at 300 K.

The excitation process of Positronium in AEGIS experiment is described in the following chapter. Here we just need to mention that the apparatus dynamics should be able to perform the excitation within 20 ns. At this time scales we can disregard the temporal decay dependence of orthopositronium that we have assumed for fitting the time of flight measurements. Actually sizes and evolution of the cloud should be investigated from the distribution $\frac{1}{t}p\left(\frac{x}{t}\right)$, i.e. accounting only for the Maxwellian diffusion from the silica surface. The average and the standard deviation with respect to the distance from the target are

$$\langle x\rangle = \int_0^\infty \frac{x}{t}p\left(\frac{x}{t}\right)dx = t\sqrt{\frac{8}{\pi}\frac{k_bT}{m}}$$

$$\sigma = \sqrt{\langle (x-\langle x\rangle)^2\rangle} = \sqrt{\langle x^2\rangle - \langle x\rangle^2} = t\sqrt{\left(3-\frac{8}{\pi}\right)\frac{k_bT}{m}}$$

The ratio of the two quantities shows that both parameters are linearly increasing with time. Thus the ratio is constant showing that the average doubles the standard deviation ($\langle x\rangle/\sigma \approx 2.37$). As consequence we define the external edge radius of the Positronium to be

$$r = 2\langle x\rangle = t\sqrt{\frac{32}{\pi}\frac{k_bT}{m}}$$

In fact we can calculate that, under the approximation conditions, 98% of Positronium atoms are contained inside the indicated distance. In this way we have found a simple relation to estimate the size of the Positronium cloud after positrons implantation.

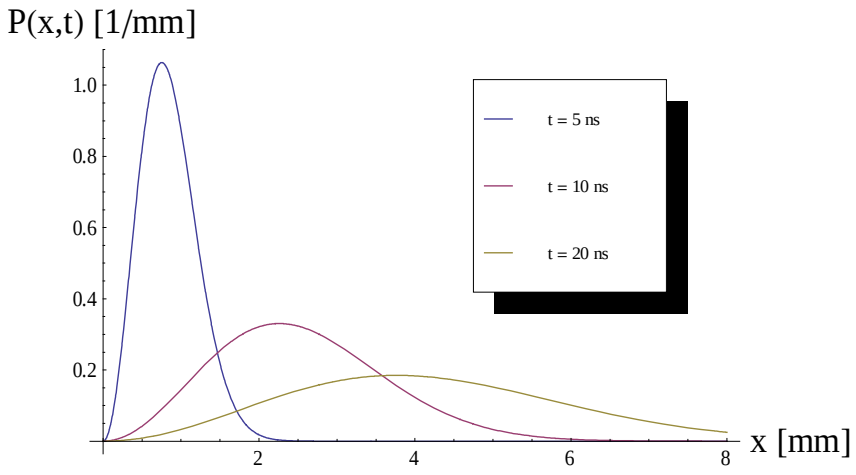

Figure 16 – Probability density function of Positronium exiting from the target with respect to the distance x from the target. Temperature value have been fixed to 1500 K. Different curve are evaluated for different delay time after positrons implantation under the silica surface

Laser Apparatus

Description

The production of antihydrogen in AEGIS experiment will be achieved mixing antiprotons with Positronium atoms. In describing the synthesis process we pointed out how the adoption of Positronium in Rydberg states enhances the reaction cross section. Laser apparatus that should excite Ps atoms has been developed and tested at the *Laboratorio di Ottica Quantistica e Laser* of *Dipartimento di Fisica* of *Università degli Studi di Milano*, in collaboration with the *Istituto Nazionale di Fisica Nucleare*. The laser system has been designed to produce pulsed light radiation at two different wavelengths. The first is an ultraviolet (UV) radiation at 205nm corresponding to the energy separation between ground state and the level with n = 3. The second is an infrared(IR) radiation ranging from 1650 nm to 1700 nm that should produce excitation to Rydberg levels starting from n = 3 [16-19].

This two-step transition is necessary to allow a practical and relatively inexpensive assembly of a laser system together with the optical system, to succeed in the efficient excitation process of Positronium atoms. In fact a direct transition from the ground state to a $n > 20$ one would require a deep UV laser radiation. At those wavelengths most of the materials commonly adopted in optics are useless, resulting opaque or scarcely reflecting. Moreover the wavelength is requested to be tunable in order to excite different Rydberg energy levels as can be required by a suitable experimental tuning. These considerations had led the group to look forward towards the choice of a two-step transition and to realize the tunable components in the infrared range.

Laser layout has been designed to fulfill the requirements of two proposed experiments in AEGIS project, in which Positronium should be excited to Rydberg levels. Before experimenting on gravity with antimatter, the excitation process of Positronium is going to be exploited in a related, but different apparatus. At the time of AEGIS proposal little was known about Rydberg levels of Positronium, so a second experiment was thought not only to pave the way for antihydrogen production, but also to investigate experimentally the energy states of the Positronium atom in the presence of electric and magnetic fields. As a matter of fact, Ps Rydberg excitation has been recently achieved using a different excitation scheme [20]. They used a two-step excitation process yet, but bringing Positronium from the 1^3S to the $2\ ^3P$ as the result of the first step. In this research they have been able to excite about 90% of a cloud of Ps atoms in the intermediate level. At that time the laser apparatus of AEGIS was in development, no experimental results were accessible to estimate the effective excitation capabilities achievable by the system, and verify simple theoretical prediction [16]. But now, looking at the experimental results obtained by Cassidy, the theoretical expectations for our case had turned out to be remarkable conservative, predicting that only the 33-60% of the atoms would be converted from the ground to the n = 3 states. Notwithstanding the fact that

the energy transition is different, we could expect in AEGIS similar result as in Cassidy experiment.

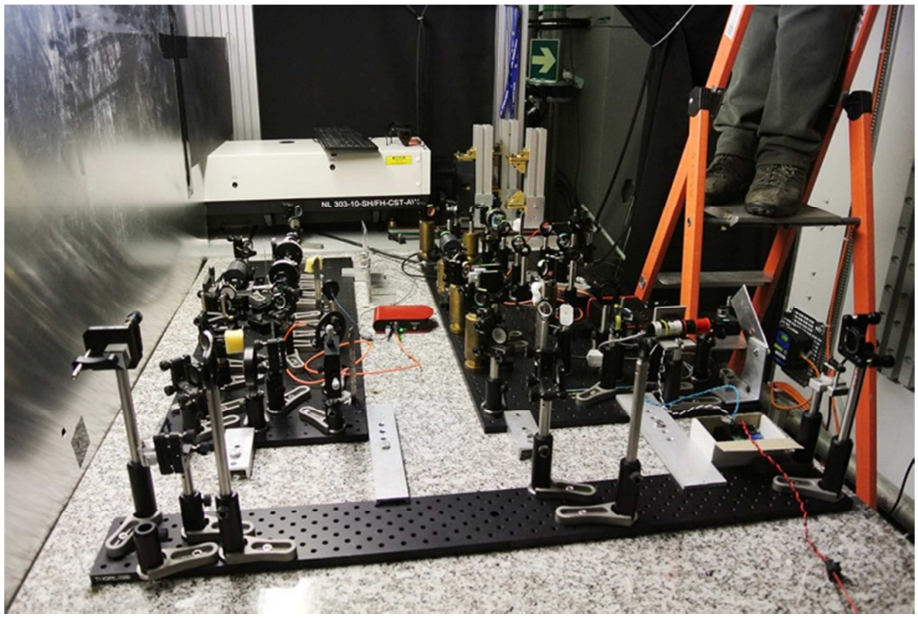

Figure 17 – Picture of the laser apparatus (February 2013)

AEGIS laser system is based on the pulsed emission of a Q-switched Nd:YAG laser which has the role of the pump to generate all the other wavelengths. Firstly, harmonic generation by nonlinear crystals is accomplished to produce laser pulses at frequencies twice and four times the original 1064 nm laser line. Secondly, nonlinear effects in crystals combine these harmonics to allow for the conversion of the fundamental frequency into the desired radiations, matching the transition energy gaps in Positronium.

The scheme of the laser system can be logically divided into four different blocks, following the layout assembled on breadboards in our laboratory (see Figure 18). The first part is the Q-switched Nd:YAG laser completed with second and fourth harmonics generation (from EKSPLA), the second and the third are two optical breadboards dedicated to the generation of UV and IR radiation pulses and the last one is dedicated to synchronization of the two pulses.

A detailed description of the apparatus up to the final wavelength generation is reported in the *Laurea Triennale* thesis of F.Ferri [18], who did the final assembly of the first three breadboards.

In what follows we will give an introduction to nonlinear optics to describe the processes adopted in AEGIS for the generation of the two excitation wavelengths. In this brief description of nonlinear optical effects we will disregarded the spectral and spatial properties of the light pulses. Actually, during the pulse release of the Nd:YAG laser, more than one oscillation modes of its optical cavity is excited, thus producing a complicated pulse spectrum of comb appearance. To obtain detailed results in predicting Positronium excitation a more accurate model of the laser was taken into accounted by F.Villa [19]. In its phd Thesis, he investigated this process with an accurate model of the laser pulse production and a detailed

description of the energy levels in Positronium. Starting from his results we will give a simpler explanation of the phenomenon, fitting the simulation trends in two-level atom approximation.

From the theoretical results regarding the interaction of light and Positronium we will extract all the necessary information that have been used in the development of the optical system for Positronium excitation. Subsequently we will describe this system explaining how the excitation is foreseen to be realized near the antihydrogen recombination region.

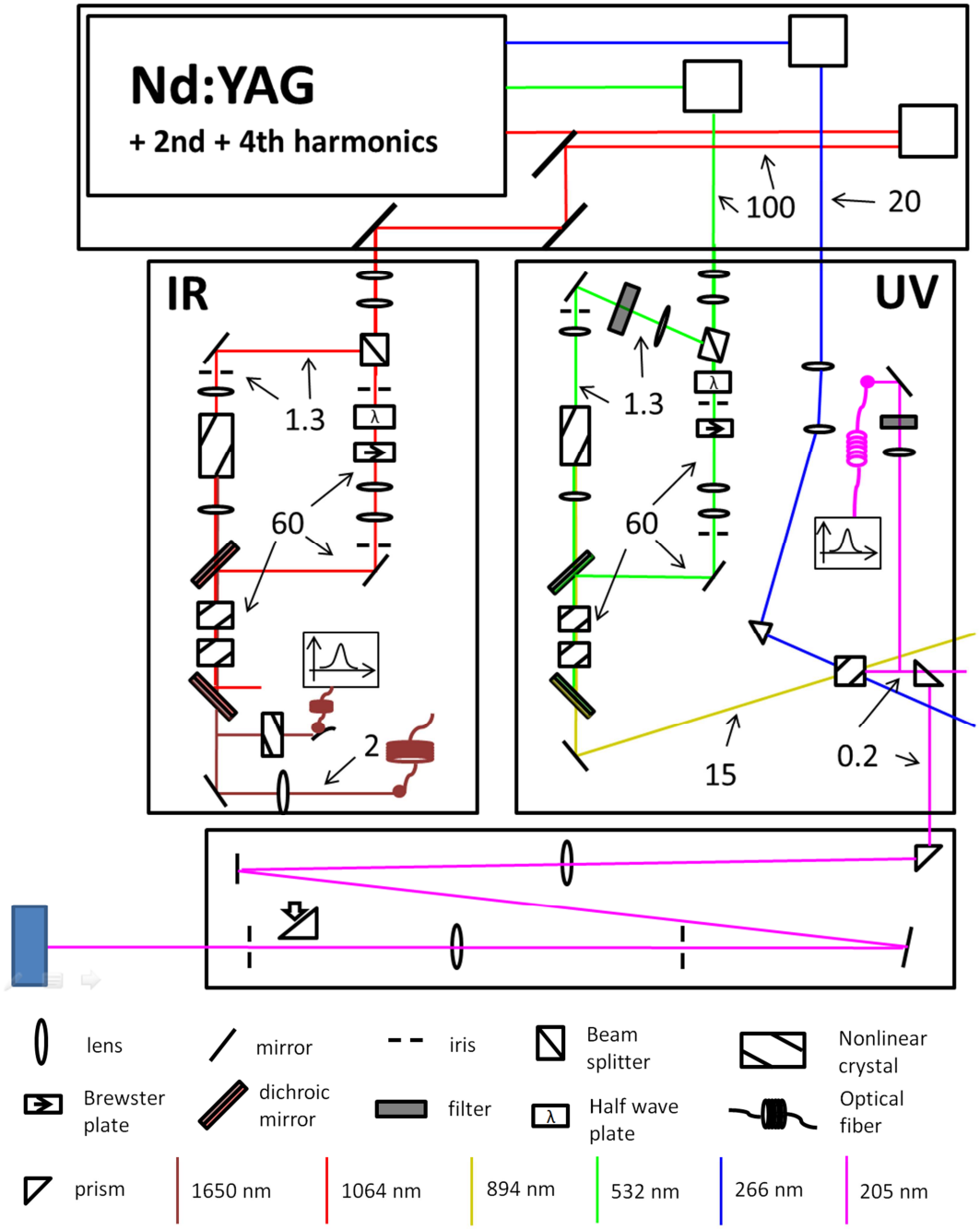

Figure 18 – Drawing of the laser apparatus. The numbers reported of the figures are the pulses energies in mJ measurable along the indicated beam lines.

Nd:YAG laser and Q-switch

The active medium of the pumping laser system is a Nd:YAG crystal. This crystal is a garnet containing Yttrium, Aluminum and Oxygen (chemical composition $Y_3Al_5O_{12}$), where almost one atom of Yttrium triply ionized over one hundred is substituted with one ion atom of Neodymium (Nd^{+++}). This type of laser can be pumped with laser diodes at 808 nm or incoherent light due to great absorbance window in the spectrum. Nd ions absorb the radiation from the external pump and get excited. The absorption bands are coupled by fast nonradiative decays to the metastable $^4F_{3/2}$ level from where the decay to the lower I levels occurs. However, decay rate of the latter is much slower (0.23 ms) than that of the former, because the transition, in the isolated ion, is forbidden via electric dipole coupling and becomes weakly allowed due to the crystal field interaction. This means that level $^4F_{3/2}$ accumulates a large fraction of the pump power and is therefore a good candidate as the upper level for lasing transition. Furthermore the strongest transition from this level is found to be toward $^4I_{11/2}$, which is then coupled by a fast (hundreds of ps) nonradiative decay to $^4I_{9/2}$ ground level; so that thermal equilibrium between these two is rapidly established. In this picture an optical wave can be amplified coherently if its frequency corresponds to the energy gap of $^4F_{3/2} \rightarrow {}^4I_{9/2}$ transition. As a matter of fact such a radiation stimulates the transition in both directions and Nd atoms in $^4I_{9/2}$ state can absorb a photon to get into the higher level. However, in the classical four-level scheme, thanks to the pump and nonradiative decays effects the density of Nd atoms in $^4F_{3/2}$ state can be easily kept greater than that of $^4I_{9/2}$ favoring the amplification process. This working condition is usually called population inversion because the density per unit volume of the ions in the upper level is greater than the density of the lower state.

If a pumped crystal of Nd:YAG is inserted in a resonant optical cavity with a small transmission mirror, the pump and the emission drain effects compensate each other, and the laser can reach a stable working condition. Essentially one has light amplification governed by stimulated emission, because photons are allowed to bounce back and forward. To operate in this Continuous Wave emission, pump energy (and population inversion) must overcome a threshold value dictated by cavity loss. The higher the loss the higher the threshold will be.

However for AEGIS purposes a pulsed regime has been preferred to generate light radiation and excite Positronium in a few nanoseconds, only when atoms are actually exiting from the silicon target. This solution allows generating light radiation only when needed and enhances the nonlinear behavior of the crystals adopted for harmonics generation.

The pulsed laser operating regime selected for this purpose is the so-called Q-switch. This regime is achieved modifying abruptly the cavity loss properties, hence changing the threshold for laser emission. The mechanism of the pulsed emission is as follows: at first photon losses are strongly enhanced in order to keep very low the rate of stimulated emission. Hence the threshold for light amplification is very high and the pump can excite as much Nd atoms as possible. When the active population has reached a desired maximum, the cavity is “switched” towards a state with very low losses, hence with a lower amplification threshold.

This change of status triggers a sudden stimulated light amplification in cascade releasing a powerful burst of light in a short while. The cavity loss change is very difficult to be obtained mechanically and normally is achieved by using special devices called optical modulators (see below).

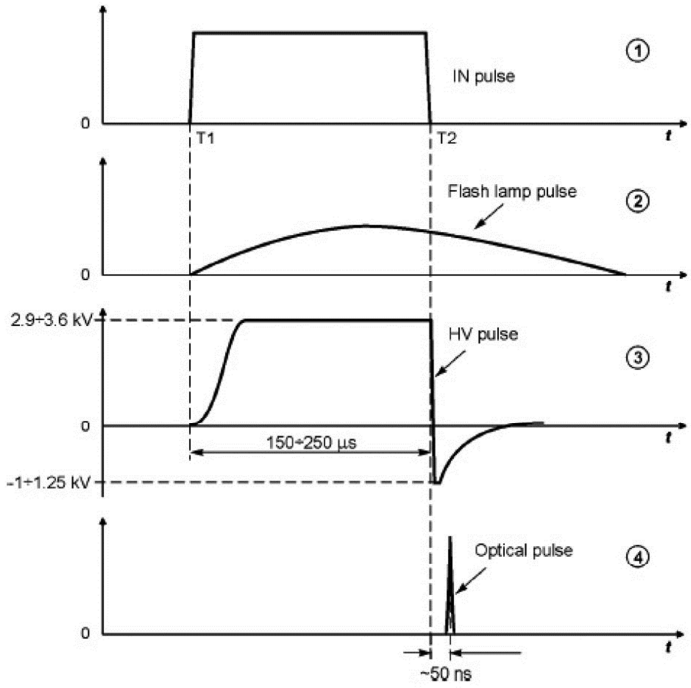

Figure 19 – Plots of physical quantities of the laser during pulse release process with respect to time. Plots are in arbitrary units when not specified. (from EKSPLA NL300 Series Laser manual). (1) Trigger electrical pulse; (2) flash lamp intensity (3) voltage applied to the Pockels Cell; (4) light pulse released from the cavity.

In this process it is not requested to release coherent light in a steady state condition and as consequence mirror design and pumping method can substantially differ from continuous wave laser. Curvature radii of mirrors in cw systems are usually chosen in order to reduce the geometrical loss of the cavity by containing beam divergence (stable cavities). This is particularly useful in containing pumping energy consumption, which must constantly compensate the exiting power. However in these configurations beam diameter end up to be pretty small, below 1/100 of cavity length, and only active media of comparable sizes are really worth to be used. In case of Q-switch regime cavity losses could and should be much higher with respect to continuous wave emission. From one side, while the stimulated emission process is precluded, the density of Nd atoms in $^4F_{3/2}$ level (upper lasing level) can greatly exceed the threshold value for cw emission, thus enabling the amplification operation for a short amount of time. Then to obtain short pulse duration loss should be suitably adjusted in order to release light quickly after the end up of the amplification process. As a consequence configuration of the resonant cavity could be unstable, as opposed to cw laser, thus opening the possibility to adopt bigger crystal and bigger cross dimensions of the output beam.

Following laser operation, pump is not supposed to act continuously too. In AEGIS laser, the active population of the $^4F_{3/2}$ level is realized by a Xenon flash lamp. With a working frequency of 10Hz the flash lamp excites the Nd ions and, when needed, it is possible to switch the status of the cavity losses to release the pulse. The 10 Hz working frequency of the lamp is necessary to heat up the cavity and the Nd:YAG, but the pulse can be released at will. The regular operation of the flash lamp reduces output energy fluctuations that otherwise would compromise the working efficiency of the entire system.

In typical operating conditions the laser generates a pulse of 5 ns length jittering, exiting the cavity after about 0.5 ns with respect to the electrical trigger signal.

The sudden change in optical cavity loss properties is achieved thanks to a nonlinear element that modifies its physical properties by application of a voltage difference. In the pictorial representation of Figure 20 this device appears like a parallelepiped closed inside two electrodes forming a plane capacitor, which control the birefringence of the medium by means of the so-called Pockels effect.

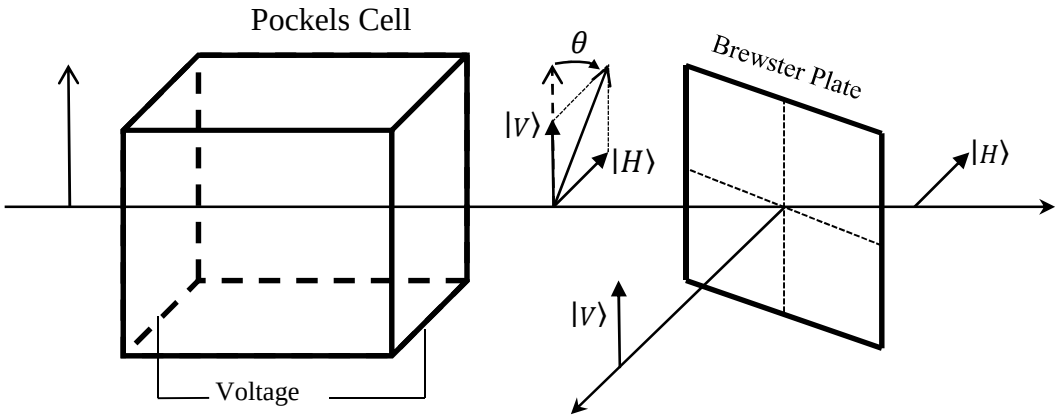

Figure 20 – Pictorial representation of the active Q-switch realized with the combined system Pockels Cell – Brewster Plate

The Pockels effect relates to the change in the refractive index of a non-centrosymmetric medium when a DC electric field is applied. Let us assume to orient the cavity of the laser in the z direction, hence having an optical wave polarized in the x-y plane. We insert into the cavity one of this special medium, specifically a uniaxial crystal with the optical principal axis coincident with z. The medium has a thickness l and a DC voltage of V could be applied between the exit and the entrance surfaces. The equation for the refraction index ellipsoid for the medium can be expressed as follows

$$\frac{x^2+y^2}{n_o^2}+\frac{z^2}{n_e^2}+2xy\frac{rV}{l}=1$$

where r is a proportionality coefficient that indicates the strength of the nonlinear effect while n_o and n_e are the ordinary and extraordinary refractive indices. In our configuration the transverse section of the ellipsoid is an ellipse whose axes are inclined at 45° to the x and y

axes. The lengths of the semi-axes, which represent the refractive indices of the two mutually orthogonal polarized fields propagating in the z-direction are

$$n_{\pm} \cong n_0 \left(1 \pm \frac{1}{2} n_0^2 r \frac{V}{l}\right)$$

The nonlinear medium therefore behaves as a wave plate, whose strength can be controlled by varying the applied voltage. The Pockels effect allows controlling electrically the polarization properties of a light beam and this is the basis principle of the Pockels cell. Using the cell as an adjustable quarter wave plate it is possible to create an optical switch, combining the polarization rotating effect with a polarization selector, like a Brewster plate. In fact, this last element allows propagation within the resonant optical cavity only for light with fixed polarization; if the polarization is rotated, light cannot propagate in the cavity but is reflected away, thus increasing cavity energy losses. The performance achievable by this type of system are very well suited for a sudden change of the loss status of a laser cavity, since the Pockels cell can switch in less than one nanosecond.

Nonlinear optics for frequency generation

Many applications of coherent radiation require light emission at a specific wavelength for spectroscopy targets. Indeed electromagnetic waves can induce a transition between two atomic states, under the assumption that the radiation frequency corresponds to the energy gap between the two levels. These requirements have lead scientists to develop several techniques in order to obtain at will radiation over a wide range of wavelengths in the electromagnetic spectrum. To achieve this goal it is possible to choose a specific active medium to generate the desired frequency, or to modify the wavelength after generation. The laser system developed in Milano adopts this second solution, starting from the energetic photons of the fundamental harmonics of Nd:YAG at 1064 nm.

Laws of classical optics can be used to reflect, convey or focus light at any wavelength, but cannot be used to convert one frequency into another. However it is possible to find some crystals in nature that shows nonlinear behavior when forced with an external electromagnetic field.

In many real atomic systems, electrical polarization P_i induced by an electric field E_i can be expressed as a Taylor series expansion:

$$P_i = \epsilon_0 \chi_{ij} E^j + 2\epsilon_0 d_{ijk} E^j E^k + \cdots$$

where the coefficients are called susceptibilities. The first coefficient is the linear dielectric response of the medium. The coefficient d_{ijk} describes a second order optical susceptibility and it is found to be totally symmetric, i.e. it is invariant under reshuffling of its subscripts. This nonlinear response gives rise to numerous interesting phenomena and can be used to transfer energy between radiation beams at different frequencies. As a matter of fact the tensor s is normally quite simple, being null for most combinations of i, j and k subscripts. As

an example we can take the two types of crystals that are currently mounted on the laser table which are KDP and BBO. The non-zero elements of KDP nonlinear tensor have subscripts $(1;2;3)$ like $d_{123} = 0.39$ pm/V while for BBO the non-null elements are $d_{112} = -d_{222} = 2.2$ pm/V and $d_{113} = d_{223} = 0.08$ pm/V and their subscript reshuffling.

A radiation wave equation depending on nonlinear terms can be obtained by expanding Maxwell equation for the curl of the magnetic field

$$\nabla \times \boldsymbol{B} = \mu_0 \boldsymbol{J} + \mu_0 \frac{\partial \boldsymbol{D}}{\partial t} = \mu_0 \boldsymbol{J} + \mu_0 \frac{\partial}{\partial t}(\epsilon_0 \boldsymbol{E} + \boldsymbol{P})$$

Using the vector potential $\boldsymbol{A}$ in Coulomb gauge ($\nabla \cdot \boldsymbol{A} = 0$) and assuming $\boldsymbol{J} = 0$ the above expression becomes

$$-\nabla^2 \boldsymbol{A} = -\mu_0 \frac{\partial}{\partial t}\left(\epsilon_0 \frac{\partial \boldsymbol{A}}{\partial t} + \boldsymbol{P}(\boldsymbol{A})\right)$$

Now, using the expansion for *P* and separating the linear expression from the nonlinear one

$$(1+\chi)\frac{1}{c^2}\frac{\partial^2 A_i}{\partial t^2} - \nabla^2 A_i = -2\epsilon_0 \mu_0 d_{ijk} \frac{\partial}{\partial t}\left(\frac{\partial A_j}{\partial t}\frac{\partial A_k}{\partial t}\right)$$

Let us assume forcing a crystal with three different waves of frequencies ω_1 , ω_2 and ω_3 . Necessary condition to mix these waves inside the crystal is to select suitable wave linear polarizations as required by nonzero coefficient of the nonlinearity tensor. Following this requirement, we can simplify all the mathematical treatment by taking polarized plane waves:

$$A_k = A_1 e^{i(k_1 z - \omega_1 t)}$$

$$A_j = A_2 e^{i(k_2 z - \omega_2 t)}$$

$$A_i = A_3 e^{i(k_3 z - \omega_3 t)}$$

Moreover we can assume that the amplitudes of the three fields are not depending on time and that they will mix each other along the whole crystal. The left hand side of the modified wave equation becomes:

$$\left(\frac{n^2}{c^2}\frac{\partial^2}{\partial t^2} - \frac{\partial^2}{\partial z^2}\right) A_3 e^{i(k_3 z - \omega_3 t)} = A_3 \left(\frac{n^2}{c^2}\frac{\partial^2}{\partial t^2} - \frac{\partial^2}{\partial z^2}\right) e^{i(k_3 z - \omega_3 t)} + \left(2ik_3 \frac{\partial A_3}{\partial z} - \frac{\partial^2 A_3}{\partial z^2}\right) e^{i(k_3 z - \omega_3 t)}$$

with similar equations for A_1 and A_2. The exponential derivatives of this relation can be simplified using the wave dispersion relation $\frac{n^2}{c^2}\omega^2 - k^2 = 0$ and we can also employ the spatial slowly varying approximation by assuming $\frac{\partial^2 A_3}{\partial z^2} \ll k_3 \frac{\partial A_3}{\partial z}$.

The nonlinear wave equation ends up:

$$\frac{dA_3}{dz} = d\ \frac{\omega_1\omega_2\omega_3}{c^2 k_3} A_1 A_2 e^{i\left((k_1+k_2-k_3)z-(\omega_1+\omega_2-\omega_3)t\right)}$$

In this expression d accounts for the suitable chosen element of nonlinear tensor d_{ijk}.

As stated by this expression, energy transfer among the amplitudes of the three fields is controlled by the phase factor $e^{i\left((k_1+k_2-k_3)z-(\omega_1+\omega_2-\omega_3)t\right)}$ that regulates the energy flow in constructive or destructive way. As a matter of fact this phase term oscillates on micrometer and picosecond scale for almost the totality of the three optical waves combination. As a consequence we observe only tiny nonlinear effect if the phase of the exponential is not sufficiently constant. In the case in which we are interested, that is generation and amplification of a signal at the frequency ω_3 by pumping with the other two waves, which in practice are nearly undepleted during propagation in the crystal, we can neglect any variation of A_1 and A_2 coefficients and assume for energy conservation that $\omega_1 + \omega_2 - \omega_3 = 0$. The amplitude difference of A_3 exiting from a crystal of length L will be

$$\Delta A_3 \propto A_1 A_2 \int_0^L dz\, e^{i(k_1+k_2-k_3)z} \propto A_1 A_2 \frac{\sin\left(\frac{k_1+k_2-k_3}{2}L\right)}{k_1+k_2-k_3}$$

From this result it is clear that if we would employ nonlinear crystal to obtain frequency conversion we must turn this oscillating behavior into a coherent and constructive effect. One solution could be to use an appropriate birefringent crystal in which the condition $k_1 + k_2 - k_3 = 0$ can be realized, hence operating in the so called phase matching condition.

Signal amplification can be profitably performed by using phase matching conditions in nonlinear crystals, but for frequency generation it turns out more efficient, for various reasons, a different method. In fact, it is possible to superimpose several layers of crystals so thin and suitable prepared to obtain an overall constructive effect in harmonics mixing.

These types of crystals are called periodically poled and their regime of operation is called Quasi Phase Matching. In practice when $\sin\left(\frac{k_1+k_2-k_3}{2}L\right)$ turn to negative amplitude variations, the light beam cross to a different layer with inverted crystallographic axes, allowing the function to start growing again. Compared with the perfectly phase-matched case, QPM leads to lower conversion efficiency if the nonlinear coefficient is the same: the effective nonlinearity d_{eff} is reduced by a factor of $2/\pi$. However, QPM makes it possible to use the same polarization direction for all interacting waves, and this often corresponds to using a stronger element of the nonlinear tensor. In AEGIS laser, for example, two periodically poled KTP crystals (PPKTP) are employed. Their birefringent phase matching (ordinary phase matching) can be exploited with d_{311} =1.95 pm/V and d_{322}=3.9 pm/V, whereas QPM normally uses the higher d_{333} =15.3 pm/V, which effectively results in 9.7 pm/V taking into account the $2/\pi$ factor. Thus using d_{333} is a significant advantage with respect to the other coefficients. A second advantage is the typical propagation direction along

a crystal axis (noncritical phase matching), so that spatial walk-off is avoided, and the acceptance angle is large. Further, the quasi-phase matching period can be adjusted in order to have a convenient phase-matching temperature. In fact the output of a precise frequency is obtained tuning crystal temperature to an appropriate value.

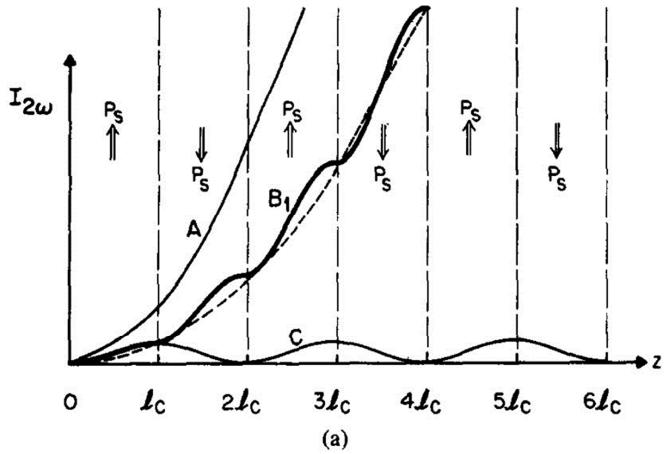

Figure 21 – Comparison between the gained intensity in phase matched (A) and quasi-phase matched (B_1) crystals with equal nonlinear coefficient. Notice the oscillatory behavior of the quasi-phase matched amplification induced by the periodicity of the crystal.

In AEGIS laser system both type of crystals are used, but we will concentrate for the mathematical treatment on the simpler case of phase matched crystal. Since d_{ijk} is a symmetric tensor the other two equations for $\frac{dA_2}{dz}$ and $\frac{dA_1}{dz}$ are essentially the same as the one for $\frac{dA_3}{dz}$. These three equations show that chosen one of the three waves, its amplitude suffer increase or decrease depending on the product of the other two waves.

Finally, with energy conservation and phase matching relation we are left with three coupled differential equations:

$$\frac{dA_3}{dz} = d\,\frac{\omega_1\omega_2\omega_3}{c^2 k_3} A_1 A_2$$

$$\frac{dA_2^*}{dz} = d\,\frac{\omega_1\omega_2\omega_3}{c^2 k_2} A_1 A_3^*$$

$$\frac{dA_1}{dz} = d\,\frac{\omega_1\omega_2\omega_3}{c^2 k_1} A_2^* A_3$$

Starting from this system we can have a brief overview over the physics of wavelength generation to excite Positronium in AEgIS.

To produce the 1650 nm radiation, corresponding to the transition between the third and Rydberg levels in Ps, a nonlinear process called Optical Parametric Amplification is used. Here the fundamental harmonic of the Nd:YAG is used as a pump for generating new waves,

one the 1650 nm and the second at 3 μm. In this process a photon belonging to pump wave A_3 is "down converted" in two photons of lower energy, corresponding to the idler waves A_1 and A_2. For this case we will assume that the amplitude of the (strong) pump is not depleted along the crystal and so we are left with the coupled differential equations

$$\frac{dA_2}{dz} = d\ \frac{\omega_1\omega_2\omega_3}{c^2 k_2} A_1 A_3$$

$$\frac{dA_1}{dz} = d\ \frac{\omega_1\omega_2\omega_3}{c^2 k_1} A_3 A_2$$

Taking the second derivatives of the second equation and substituting the result into the first we obtain a second order differential equation with constant coefficient:

$$\frac{d^2A_1}{dz^2} = \left(d\frac{\omega_1\omega_2\omega_3}{c^2}A_3\right)^2\ \frac{1}{k_1 k_2} A_1$$

The solution of the differential equation for A_1 indicates that the amplitude undergoes an exponential grow and we find the following result as a function of the length L of the crystal:

$$A_1 \propto \sinh\left(d\ \frac{\omega_1\omega_2\omega_3}{c^2\sqrt{k_1 k_2}} A_3 L\right)$$

The differential problem was solved assuming a suitable initial condition for the signal amplitude. In particular the process is called Optical Parametric Amplification (OPA) when an amplification of a preexisting harmonic field is performed. If the initial field is negligible, as in the case in which only quantum vacuum fluctuations are present, the process of creating new waves using this nonlinear effect is called Optical Parametric Generation (OPG) and should be investigated in quantum approximation, to correctly evaluate the energy fluctuations of the new waves.

In AEGIS laser system the OPG of the 1650 nm is achieved by using a periodically poled crystal. Unfortunately periodically poled media have lower damage threshold than ordinary crystals. As consequence the harmonic buildup has to be realized in two-step adopting different type of materials. First the OPG generates a pulse seed that subsequently is amplified with an OPA system made by two KDP crystals. This solution, compared with that of a single crystal system, has the advantage to reduce the signal to noise ratio of the output pulse. In fact field fluctuations during the amplification process are proportional to the square root of the number of photons that composes the pulse. Thus OPG systems, working at low light intensities suffer from fluctuations of quantum nature, but the subsequent amplification depress this secondary effect.

The apparatus that generates the 205 nm radiation used for the first transition of Positronium can be summarized as follows. The second harmonic of the laser is used in an OPG-OPA system, with the same scheme employed in the infrared subsystem described above, to create a 894 nm radiation. The 894 nm is combined with the Nd:YAG's fourth harmonic building up a 205 nm radiation pulse via frequency sum process (SFG). Thus at the

end of the UV breadboard two photons belonging to a 894 nm and 266 nm beams are “up converted” to generate a more energetic photon at 205 nm.

In this case we model the generation process by considering two beams of amplitude $A_1 = A_{10} - \delta A_1$ and $A_2 = A_{20} - \delta A_2$ and wavelength $\omega_1 = 266\text{nm}$ and $\omega_2 = 894\text{nm}$ to obtain a pulse at 205nm using a BBO crystal. A_{10} and A_{20} are the values of the fields at the entrance of the crystal, while δA_1 and δA_2 accounts for small amplitude depletion inside the medium. The differential equations for nonlinear crystals can be expanded in this approximation disregarding all the second order terms like $A_1 \delta A_2$, $\delta A_1 A_3$ and $\delta A_2 A_3$.

$$\frac{dA_3}{dz} = d\ \frac{\omega_1 \omega_2 \omega_3}{c^2 k_3}(A_{10}A_{20} - \delta A_1 A_{20} - A_{10}\delta A_2)$$

$$\frac{d(\delta A_2)}{dz} = -d\ \frac{\omega_1 \omega_2 \omega_3}{c^2 k_2} A_{10} A_3$$

$$\frac{d(\delta A_1)}{dz} = -d\ \frac{\omega_1 \omega_2 \omega_3}{c^2 k_1} A_{20} A_3$$

Differentiating the first equation and simplifying we get:

$$\frac{d^2 A_3}{dz^2} = \left(d\ \frac{\omega_1 \omega_2 \omega_3}{c^2}\right)^2 \frac{1}{k_3}\left(\frac{1}{k_1}A_{20}^2 + \frac{1}{k_2}A_{10}^2\right) A_3$$

The first and second order equations should be combined together to obtain for the generation of A_3

$$A_3 = \frac{a_1 A_{10} A_{20}}{\sqrt{a_3(A_{10}^2 a_2 + a_1 A_{20}^2)}} \sin\left(L\sqrt{a_3(A_{10}^2 a_2 + a_1 A_{20}^2)}\right) \qquad (2)$$

with $a_j = d\ \frac{\omega_1 \omega_2 \omega_3}{c^2 k_j}$

This result, obtained in low depletion approximation, have been used to fit the output power of the 205 nm as a function of the pulse power of the fourth harmonics of the laser as shown in Figure 22.

If in the SFG the pump waves are oscillating at the equal frequencies, the nonlinear effect is called Second Harmonic Generation, but its mathematical description does not change with respect to SFG. In this experimental scheme only one radiation is needed rather than two and the nonlinear output is the “second harmonic”: the wave that oscillates at double frequency with respect to the fundamental. In AEGIS system SHG is used to convert the 1064nm radiation into the second and fourth harmonic. Two KDP crystals are placed near the Nd:YAG laser cavity, the first one to generate the green pulses at 532 nm which is then used to obtain pulses at 266 nm.

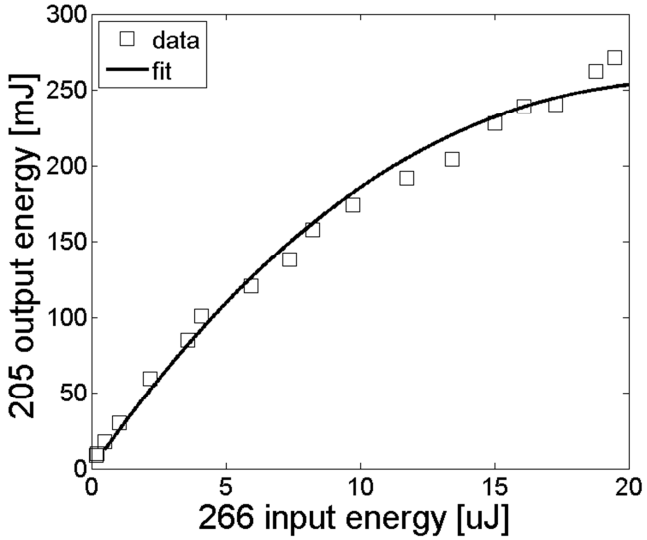

Figure 22 – Power output of the 205 nm pulse with respect to the incident power of the 266 nm. The continuous curve is obtained by a fit using (2), taking energies as squared amplitudes. In the fit only values of the input and output powers have been used as they are reported of on the plot.

Positronium excitation

Light Interaction with Positronium

Thus far we have discussed about the nonlinear effects that are adopted to generate the correct wavelengths for Positronium excitation. However we have always imagined that the laser was working only on one frequency and the Positronium cloud is accepting only one plane wave to stimulate the transition. This of course is not the case occurring in the real experiment. From one side it is not possible to produce pulsed light with spectrum restricted to only one frequency, as it is against the uncertainty principle of Fourier transform. Furthermore the Positronium exiting from the silica target will perceive a Doppler shift of the incoming light due to its motion component in light direction. Finally we need to estimate the power that the pulses have to release to the cloud; indeed we should expect that the saturation of the transitions for Positronium excitation will be favored using a suitable intense beam rather than with few photons.

For this reasons it is necessary to present some results about the interaction of light with Positronium, to show the requirements the laser system must fulfill. The core theoretical results on Ps excitation are reported in [19] and [16, 17]. Here we show their conclusions reducing the excitation model within the framework of a two-level atom system. The model is hence adopted to link laser pulses power to excitation probabilities.

Excitation of Positronium is strictly depending on generated wavelengths that should be tuned according to the atom energy transitions among levels. As a matter of fact we have found in the previous chapter a relation for the energy levels in hydrogen-like approximation, and we can use it to establish the frequency of light that stimulates the transition between the ground level and the family of levels with n = 3:

$$\nu = \frac{E_3 - E_1}{h} = \frac{1}{18}\frac{m_e q_e^4}{h^2 \epsilon_0^2} \approx 1.4622 \cdot 10^3\ THz$$

The corresponding wavelength in vacuum associated to this frequency is 205.026 nm . However the energy band to cover a Doppler broadening of the line at 100 K is $4.4 \cdot 10^{-2}$ nm (FWHM) corresponding to 300 GHz. Broadening due to Motional Stark effect for the transition 1→3 is negligible in respect to the Doppler broadening.

Positronium exiting from the target is expected to be randomly directed, thus having a momentum spread along the incoming light path, which is parallel to the target surface. This motion is the relevant component of the speed that has to be evaluated for the Doppler broadening of the transition. To be precise, Positronium beam involved in antihydrogen synthesis represents only a part of the full cloud, those directed under a very little solid angle in the region where the antiprotons are trapped. Thus the Doppler broadening to be considered

could be reduced by a factor of ten. On the other hand the laser is going to be used in other experiments within AEGIS, like to investigate Rydberg levels of Positronium. Therefore the radiation is designed to cover the entire Doppler broadened line accounting for a random scattering of Positronium departing from the silica target surface.

The correct light intensity for transition saturation of the Ps cloud can be derived with a suitable model for incoherent excitation of a simple two-level system. In our approach to the problem we will consider the flux ϕ of the incoming photons as constant in time. Stimulated transition between levels is due to the intensity if incoming light weighted by Einstein B coefficient. We will call n_1 and n_2 the population densities of the ground state and the excited state respectively, that sum up to Positronium total density $n = n_1 + n_2$. We can write the rate equations of the combined two-level system as:

$$\frac{dn_1}{dt} = B\phi n_2 - B\phi n_1 = B\phi(n_2 - n_1)$$

$$\frac{dn_2}{dt} = B\phi n_1 - B\phi n_2 = B\phi(n_1 - n_2)$$

where we neglect spontaneous emission. The difference between the two differential equations gives:

$$\frac{d}{dt}(n_1 - n_2) = -2B\phi(n_1 - n_2)$$

Starting at $t = 0$ with a completely unbalanced situation, where the total density n is in the ground state ($n_1(0) = n$ and $n_2(0) = 0$) we obtain

$$n_1 - n_2 = n\, e^{-2B\phi t} \quad \Longrightarrow \quad n_2 = \frac{n}{2}\left(1 - e^{-2B\phi t}\right)$$

Assuming constant intensity and uniform density, the probability to find a Positronium atom at excited level after a time t is:

$$p = \frac{1}{2}\left(1 - e^{-F/F_{sat}}\right)$$

To keep the formula simple we have expressed the probability as a function of the fluency F that is the energy released by pulse per unit area. The formula assumes the existence of a saturation value for the fluency F_{sat} that fixes the exponential behavior of the probability. In the case of the two-level system when $F = F_{sat}$ this probability is 43%. For systems having more than two levels, the coefficient 1/2 in front of the expression may have bigger values favoring the excitation process.

Simulation of excitation process performed by Fabio Villa was realized taking into account more complex experimental situations. His results for the transition 1→3 are represented in Figure 23. In this model the laser radiation have been simulated from generation into the cavity passing through all nonlinear crystals, while Positronium energy levels have been split according to Zeeman and Motional Stark effects. Simulation has been realized using a

Gaussian beam of FWHM of 3 mm. As a consequence the plot is expressed as a function of the total pulse energy, while E_{sat} is the energy saturation value extracted from the fit. The good approximation of the fit suggest that the results of the simple two-state model can be extended to more than two levels adjusting the overall multiplicative constant; that in the two-state system was fixed to 1/2 .

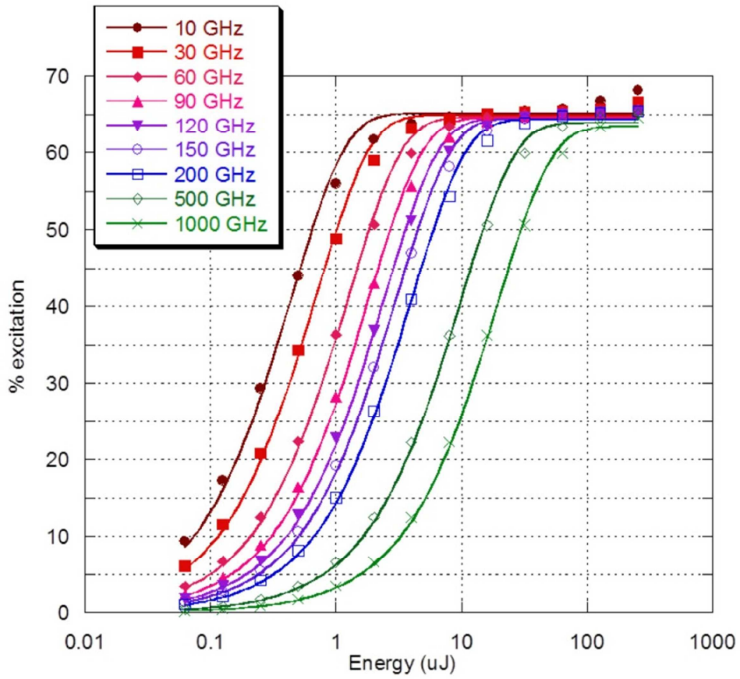

Figure 23 – Result of simulation with a detailed model for the Ps transition from ground to third excited levels. The plot shows the maximum percentage of Ps excited for different laser linewidths. Simulation assumes a 1T magnetic field, $5{\cdot}10^4$ m/s Ps velocity, laser pulse with a FWHM of 3 mm. The interpolating functions are best fit with an exponential saturation proportional to $(1-\exp(E/E_{sat}))$, i.e. the same trend of the two levels system.

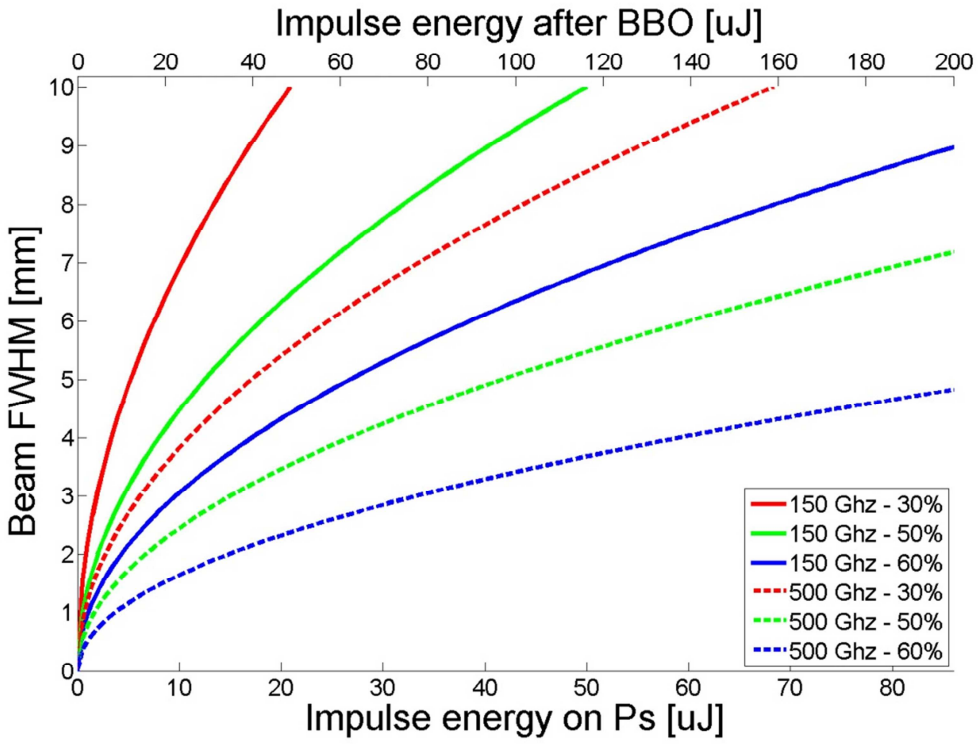

Figure 24 – The graph shows isofluency curves with respect to pulse energy and FWHM of the beam in Positronium region. Values of the fluencies are chosen to match various excitation probabilities for two different values of the linewidth, as specified in the legend. The above scale is reported for an easy-to-use read out of the plot. It indicates the energy of the 205 nm pulse measured after the generation crystal.

Figure 24 is obtained reorganizing data presented in Figure 23, and describes the interrelations between among pulse energy, line bandwidth, spot size and excitation percentage.

The results about Positronium excitation show that the spectral window of the 205 nm pulse is a critical quantity in predicting the excitation percentage of Ps. For this reason a careful study of this linewidth has been done during the assembly of the laser system [18] determining upper and lower limits for its value:

$$120\ GHz < \Delta_{\lambda 205} < 300\ GHz$$

These limits come from mathematical arguments and from a direct measurement. The spectrometer used for laser tuning performs measurements of the radiation wavelengths in air. Air's index of refraction is little, but not null, and disregarding its value lead to a frequency bias of

$$\Delta\nu = \frac{c}{\lambda} - \frac{c}{n\lambda} = \nu\left(1 - \frac{1}{n}\right) \approx 428\ GHz$$

This is a value 3-4 times bigger than the linewidth boundary values and greater than the Doppler broadening for the transition. This makes the correction worth to be considered. The corrected value for the wavelength that must be set for the SFG of the ultraviolet is:

$$\lambda^* = \frac{c}{n\nu} = 204.966\, nm$$

In the case of transitions from n = 3 to Rydberg levels the energy gap is particularly influenced by the Motional Stark effect and so the frequency broadening of the electromagnetic field cannot be calculated with the simple formula we used in the case of the transition 1→3. At 100K, with a magnetic field of 1T, the structure of the possible transition energies is almost continue with a broadening of about 10 nm (1 THz): a linewidth much bigger than due to the Doppler broadening effect (≈ 0.044 nm). From detailed simulations of the transition the saturation fluency has been calculated to be $F_{sat}(n \to \text{Rydberg}) \approx 0.98\, mJ/cm^2$. Actually for n > 16 states the saturation fluency for the transition is slowly depending on n and on the impulse duration and this dependence can be disregarded in first approximation. The bandwidth range from 1 to 4 nm has been chosen as a compromise solution to obtain both maximum excitation of Ps and concentration in a few final states.

Synchronization

To obtain excited Positronium it is necessary that light pulses cross at best the Positronium cloud that is exiting from the silica surface. Hence there are both geometrical and temporal constraints that should be considered in developing the laser and the Positronium generation apparatus.

The flash lamp of the Nd:YAG master laser works in the range of frequencies between one to ten Hz. As a matter of fact the combined system lamp-rod produces stable pulses within 5% energy pulses after held to working regime for over half an hour. For this reason the timings of the flash should be as much regular as possible and furthermore they cannot exceed the 10 Hz frequency. On the other hand once the positrons are stored in the trap they have no practical timing constraints and can be fired at will towards the silicon target. These facts lead to the necessary conclusion that the flash lamp repetition rate should be the master clock for the experimental timings.

The problem of the synchronization circuit is described in details in the parallel master thesis of Ruggero Caravita, here we will report only the key features of this trigger circuit that has been used in the development of the optical system.

The project of the circuit is based on a few signals exchange between the positrons apparatus and laser system to activate the Pockels Cell, i.e. to release the pulse at full energy only when positrons apparatus is ready to shoot. When positrons are ready (rising edge signal in input to the circuit) two signals are generated, one for the Pockels Cell and one for the positrons trap. As mentioned, the master clock of the flash lamp is fixed, so the signal directed to the laser is synchronized to this clock and is regulated to release the pulse at full

power. In the meantime the signal to the positrons trap is released too, but in this case the rising edge can be anticipated or postponed with respect to the master clock. The precise value of the delay is digitally adjustable and will be regulated while realizing the experiment.

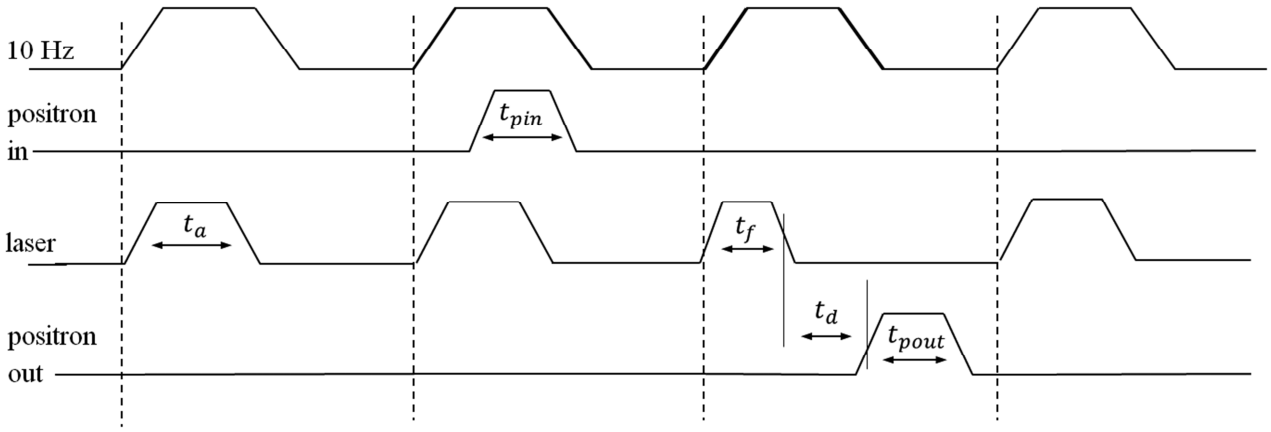

Figure 25 – Timing diagrams of the laser trigger. t_d is the tunable delay time between laser output and signal directed to positrons' trap and can be adjusted with 2 ns precision. All timings can be regulated at will with 8ns precision, but t_a and t_f are adjusted to obtain respectively none or full power of the pulse.

For the development of the optical system it is necessary to consider the jitter of both laser and positrons apparatus with respect to the trigger signal. This fluctuation in the dynamics should be compensated with the optical system. If necessary the beam spot near the silica surface should be adjustable to cover all the tolerances. However the positrons trap of AEGIS has not been tested yet and we only have a rough estimation of 5 ns. On the other hand we had the opportunity to measure the jitter of the laser pulse release. Our measurement performed with a 1 GHz oscilloscope shows that the pulse is stable below nanosecond precision with respect to the electronic trigger edge. Thus we have considered this uncertainty negligible for the purpose of the optical system project.

Optical system for Positronium excitation

Excitation of Positronium is foreseen to happen in the central region of the experiment that cannot be accessed directly with any laser radiation. The silicon target for Positronium production and the recombination trap are placed at the center of a cylindrical magnet and nothing is allowed to pass through its coils. As a consequence cables, scintillating fibers and light are constrained to bypass this obstacle in order to get in the central region. In particular the access to the inner part of the experiment is provided by two concentric flanges placed between the experimental regions of the 5T and 1T magnets. The first flange separates the room environment with the first pre-vacuum layer held at liquid nitrogen temperature and at 10^{-6} mbar, while the inner flange separates this pre-vacuum chamber with the Ultra High Vacuum region at 4 K and 10^{-10} mbar.

To get through the two flanges and constrain laser pulses to the central region we developed two different optical systems. The projected optical paths are aimed both to transfer and to synchronize the infrared radiation with the ultraviolet light. The IR pulse is guided with one optical fiber. The fiber has an FC connector on the side of the table and get to the central region thanks to two “feedthroughs”, one for each flange. The UV instead is brought near the silicon target in free propagation, using prisms to change the beam direction like done by mirrors in ordinary applications. This pulse gets to the UHV region on the horizontal plane through two viewports (type 63CF).

In the following paragraphs we will describe first the optical system of the infrared radiation. Than we will show the experimental results that led to the development of a second and different transfer line for the ultraviolet. Finally we will give the description of the optical solution adopted for the 205 nm radiation, discussing the synchronization between the two pulses.

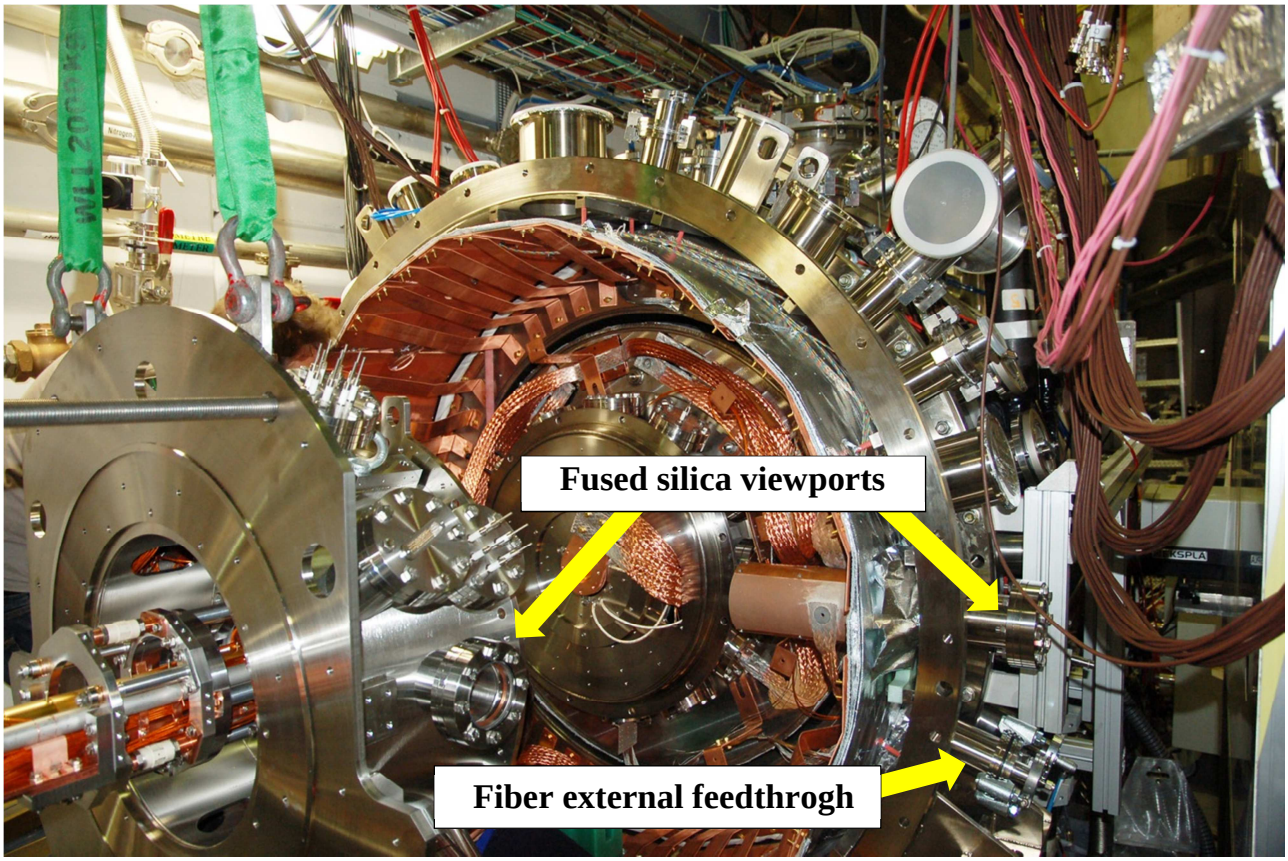

Figure 26 – Picture of the communication flanges with the central region during the assembly. The crane is holding the trap from the internal flange. Since the fiber has to be inserted from outside and cannot be pre-mounted the crane must hold the trap during the entire operation.

Transfer line for the second transition of Positronium

The infrared radiation is needed to excite Positronium from the third energy level to Rydberg levels. The description of the infrared transport should follow that of the UV needed for transition between ground and n = 3 levels, but for the purpose of explanation will be described first. Typical wavelengths corresponding to this transition are in micrometer range (≈1650 nm). At these wavelengths the absorbance and transitivity of the standard optical components are very reliable, allowing solving the transport problem with many different solutions. Among the various possibilities we have chosen to guide the infrared light by an optical fiber. As a matter of fact an optical fiber seems to be well accommodating for the needing of the experiment. From the optical table to the central region fiber can bend the light path thanks to its flexibility, bypassing the magnet with low requirements. Moreover the alignment could be controlled only on the optical table disregarding the apparatus movement during the assembly operation. Indeed the correct alignment is realized on the optical table directing the beam at the entrance of the fiber through a focusing lens.

This fiber is going to work in the wavelengths range between 1600 and 1700 nm. Since we only need power transfer without stringent characteristics on the pulse, we adopted a multimode fiber choosing the cross section dimensions as a good compromise between the damage threshold and flexibility. Thicker fibers have higher damage threshold, but they lose in flexibility being limited in the radius of curvature. We have adopted a fiber sold by Thorlabs company model FG273LEC. Further details about the physical quantities of the chosen fiber are shown in Figure 27.

From the optical table to silicon target only one continuous fiber is used. After the assembly of a 220 cm fiber only 20-30 cm exists from the external flange, sufficient enough to arrive on the optical table. There a double FC connector is installed to join a second fiber, 15-30 cm in length, which is used for the alignment. The end of the short fiber is coupled to the infrared radiation through a focusing lens (f = 10 cm) with the help of a translational stage; in this way the head can be moved in the plane orthogonal to beam looking for maximum coupling efficiency. Indeed the optimal coupling condition is recognized thanks to the fiber junction. In fact the position of the short fiber is adjusted while measuring the power output on the opposite side. After the maximum condition is realized the two fibers can be connected together. This double fiber path is thus useful for the alignment, and is adopted although it introduces a 10% power loss in the junction. Consequently the overall transmission coefficient of the line is 25%.

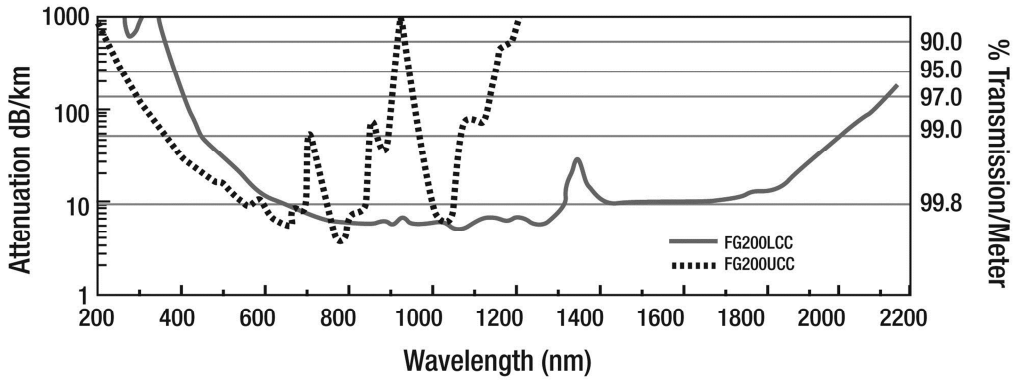

Visible-to-NIR Transmission (Low OH)

ITEM#	CORE DIAMETER	CLADDING DIAMETER	BUFFER DIAMETER	COATING DIAMETER	NUMERICAL APERATURE	MAXIMUM POWER CAPABILITY		MAXIMUM CORE OFFSET	BEND RADIUS SHORT-TERM LONG-TERM	STRIPPING TOOL See Page 862
						PULSED[a]	CW[b]			
FG200LCC	200 ± 8 µm	240 ± 5 µm	260 ± 6 µm	400 ± 30 µm	0.22 ± 0.02	1.0 MW	0.2 kW	5 µm	9 mm / 18 mm	T12S18
FG273LEC	273 ± 10 µm	300 ± 6 µm	325 ± 10 µm	420 ± 230 µm	0.22 ± 0.02	2.0 MW	0.4 kW	6 µm	11 mm / 22 mm	T12S18
FG365LEC	365 ± 14 µm	400 ± 8 µm	425 ± 10 µm	730 ± 30 µm	0.22 ± 0.02	3.4 MW	0.7 kW	7 µm	20 mm / 40 mm	T21S31
FG550LEC	550 ± 19 µm	600 ± 10 µm	630 ± 10 µm	1040 ± 30 µm	0.22 ± 0.02	7.6 MW	1.5 kW	9 µm	30 mm / 60 mm	T28S46

[a]Based on 5 GW/cm² for 1064 nm Nd:YAG laser with 10 ns pulse length and input spot size equal to 80% of the core diameter

[b]Based on 1 MW/cm² for 1064 nm Nd:YAG laser and input spot size equal to 80% of the core diameter

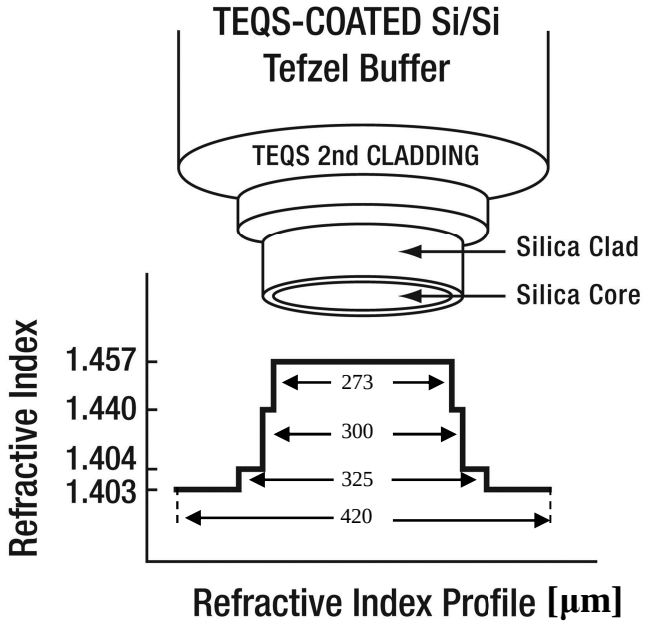

Figure 27 – We have adopted a fiber sold by Thorlabs company model FG273LEC. The attenuation curve of interest is of FG200LCC. Table and figure are taken from Thorlabs catalogue with minor modifications.

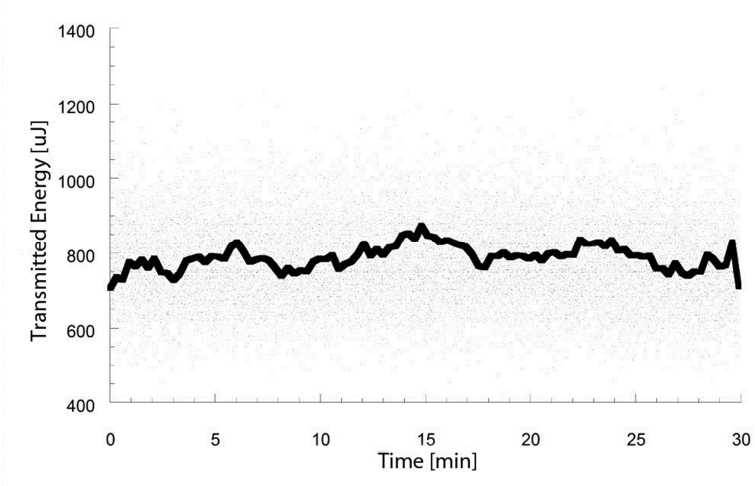

Figure 28 – Measurement of the fiber efficiency in IR pulse transmission with respect to time. Laser pulse emission was at 10 Hz repetition rate. Reported from [18].

The transmission coefficient of the line has to be considered remarkably stable because only a few optical surfaces are involved. This fact reduces the attenuation effect of dust and therefore the optical system requires only a few maintenance works. However aside these advantages the installation of the inner fiber turns out to be complicated by the assembly procedure of the two cylindrical flanges. From one side the fiber has an FC connector which forces the installation to be executed from the optical table to the central region. During the assembly the fiber is passed first in the outer flange; then into the second flange; after that is arranged the bypass of the magnet to finally reach the Ps excitation region going parallel to the trap. Obviously the inner and the outer flange are supposed to be moved one with respect to the other during the assembly operation of AEGIS, but the fiber introduces a fragile link between the two that cannot be easily removed. As a matter of fact for the assembly purpose all cables that gets to the central region are split in two, one group go from the inner flange to the trap and the others complete the cabling till outside. Moreover the inner flange supports mechanically the trap so that, when everything is installed, the crane of the AD Hall can drop the entire piece near the 5 T apparatus, where the flange is going to be screwed on. However this fixing operation occludes the experimental region where the bypass of the magnet should be arranged. At the end all this happening leaves only one possible situation to perform the installation of the fiber. It is installed when the crane is holding the trap in the experimental region near the 5 T magnet. In this case both flanges are sufficiently close for the fiber to complete the entire path, and it is possible to guide the fiber completely from outside to the central region.

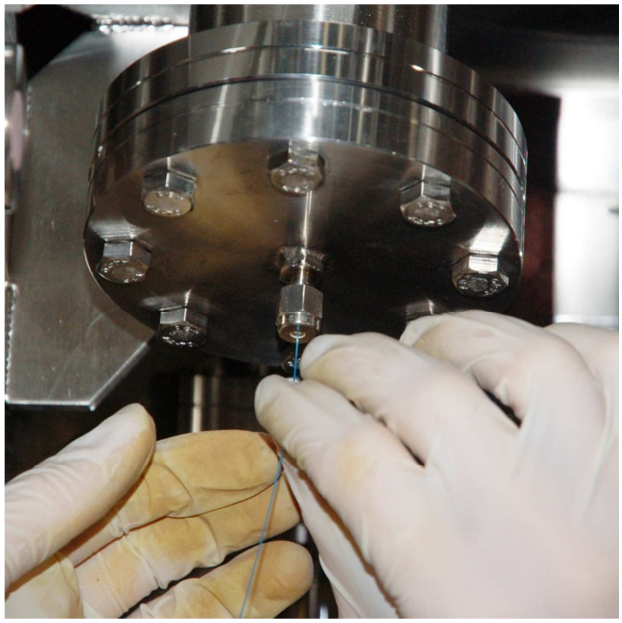

Figure 29 – Flange with feedthrough for optical fiber

The optical fiber is held near the silicon target with an aluminum fixed support. This support was designed to hold three fibers directed towards the Ps cloud. However during the assembly operation the lower fiber support has been removed due to interference with the positrons beam line. For the assembly the fiber head is pre-mounted along the axis of a cylindrical bar of 2 cm length; where the fiber is fixed by a thin elastic metal slab. The cylinder is then locked on the holder by a screw so that the fiber head is hold at the appropriate distance from the target. This distance is chosen to obtain the correct size of the spot on the Ps cloud. The numerical aperture 1650 nm laser radiation have been measured to be almost one half of the value in the datasheet. The divergence of the exiting beam is such that after 1 cm from the head of the fiber the FWHM is of 3 mm. Hence during the installation care should be taken to fix the fiber at the desired distance in order to adjust the spot sizes on the Ps cloud. Like the ultraviolet the excitation effect of the infrared light can be modeled as a transition between two energy states with saturation fluency of 0.98 mJ/cm^2 . Thus the laser output power should be regulated to overcome this fluency value considering the actual FWHM of the beam near the Si target.

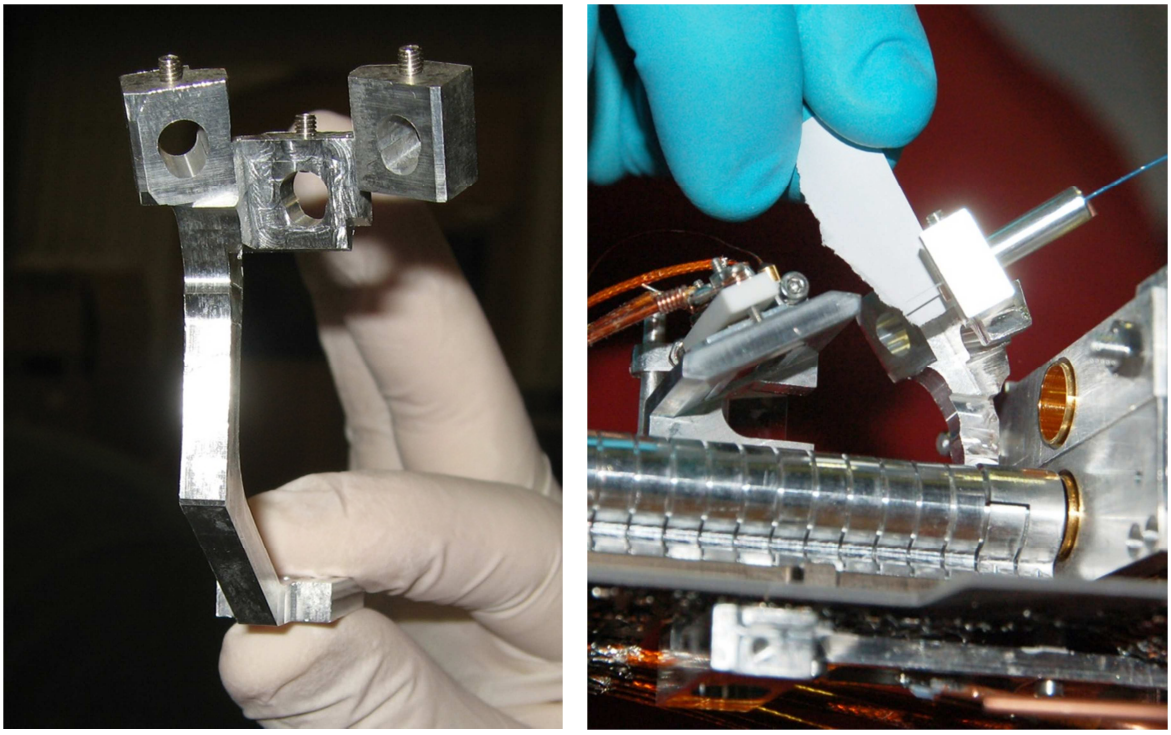

Figure 30 – Holder to fix fiber position near Positronium excitation region

For the purpose of synchronization of UV and IR pulses we measured the delay introduced by the fiber. The delay in fact is used for calculating the length of the entire optical path for the infrared branch so that infrared and ultraviolet arrive contemporarily on the Positronium cloud to obtain the two-step excitation. To measure this quantity we measured the signal acquired by a photodiode with respect to the reference electric signal used to trigger the pulse release by the laser cavity.

The jitter between the electric signal and the pulse release has been measured to be of about 0.5 ns so to reduce the uncertainties measure we have averaged the results over many pulses for each acquisition. In this way the greater systematical error belongs to the position uncertainty of the photodiode of about 1-2 cm. We took the time of flight of the pulse before and after a 220 cm fiber measuring a propagation speed of 21 cm/ns. This value combined with the systematical error estimation lead us to an equivalent index of refraction of 1.43 ± 0.1 obtained dividing the speed of light in vacuum with the measured velocity. The index of refraction of fused silica at our wavelengths (26 °C) is 1.44, thus consistent we the measured value. In our estimation no correction for the group velocity has been taken into account, since it is smaller than the uncertainty.

Optical fibers for UV

In the original project of the optical system fibers would be adopted to transfer both infrared and ultraviolet radiation. However during our experimental tests we found out that for the wavelength of the transition 1→3 an optical fiber would not fulfill the requirements of AEGIS. In fact at this wavelength fibers show a strong nonlinear absorption behavior with respect to input energies, which is worsening in time due to the degradation of the coupling region between light and silica. In this paragraph we will present the measurements performed over optical fibers with the aim of realizing the transfer for the ultraviolet pulse. We will show that fibers in this case do not meet the requirements of AEGIS forcing us to develop a different set up.

Previous studies on optical fiber that can be found in literature [21] have shown a great absorbance of fused silica fiber in the range of frequencies of transition 1→3 of Positronium. The measurement reported by Karlitschek shows how fibers absorb light with an intensity dependent trend and that the transmission coefficient reduces dramatically after a few thousand pulses. He was allowed to recover part of transmission coefficient with an annealing of the fiber, but of course this could not be a feasible solution in AEGIS; since the fiber should bring the UV radiation into a temperature controlled environment at only 4 K. We will find that observed features in our apparatus are consistent with the model proposed in the cited paper.

Fiber transmission coefficient lowers its value with respect to three different parameters: adopted intensity, high repetition rate and degradation of the coupling region between light and fiber. Dependency over intensity is due to double photon absorption, while the transmission behavior with respect to usage can be explained with formation of color centers into fiber's material. This process rapidly reduces transmission properties of fibers with respect to the number of transferred pulses. In fact for our frequencies range transmission goes to zero within 10000 transferred pulses of hundreds of μJ and of 10 ns in duration. However color centers appears to be unstable and the properties of the fiber can partially recover after annealing. The two-photon absorption causes nonlinear intensity dependence in the transmission coefficient and so that the greater is the energy input the fewer is the transmission coefficient.

Aside to these effects a further drawback can be recognized by multiple pulse transfer. In fact fibers undergo an irreversible degradation of coupling region with usage. Reasons of this effect can be threefold as a consequence of respective size between fiber core and beam spot dimensions. If the beam is too focused it can exceed damage threshold of silica. Otherwise beam could be yet smaller than the core and fiber get damaged just behind the surface. In this situation only a few modes of the fiber are excited, so that light is not being distributed so fast across the whole core diameter and local intensity maxima may occur. Finally using beam spot greater than fiber core, or coupling light in offset with respect to the principal axis, fiber get damaged at the core-cladding interface. This latter degradation is partially reversible: the fiber can recover avoiding usage for a certain amount of time.

In [18] is reported a measurement for the degradation of the coupling region with fiber of 200 cm. Acquisition was at 10 Hz repetition rate until the degradation effect was appreciable using the whole fiber length. Then the fiber head was removed reducing fiber's length for about 10 cm. Measurable transmission coefficients obtained at the beginning and after the fiber cut are comparable to each other as shown in Figure 31.

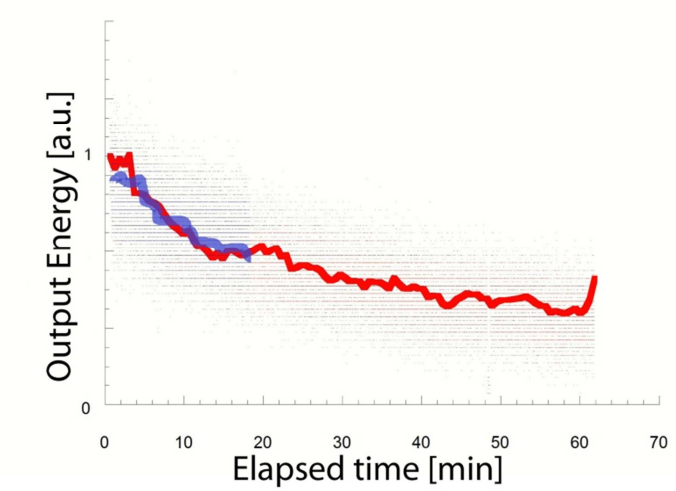

Figure 31 – Experimental result of power of 205 nm radiation transmitted with respect to time. Laser was working at 10 Hz repetition rate. Red line is obtained with a 200 cm fiber, while Blue is realized using the same fiber after removal of the first 10 cm.

To confirm the hypothesis of the two-photon absorption we have recollected the measurement reported in [18] that were obtained for different fiber lengths. In Figure 32 are reported the experimental curve for the transmission efficiency of the adopted optical fiber. As suggested this measurements shows a nonlinear trend in the transmission coefficient with respect to the intensity. We can model this behavior assuming that the intensity I variation per unit length x is given by

$$\frac{dI}{dx} = -(\alpha + \beta I)I$$

where α and β are constant coefficients. The above relation can be integrated over fiber length to obtain an equation for transmitted intensity I as a function of coupled intensity I_0 .

$$I = I_0 e^{-\alpha x}\left(1 + \frac{\beta I_0}{\alpha} e^{-\alpha x}\right)^{-1}$$

In Figure 32 are shown the fit results for nonlinear behavior of fibers changing length of the sample. From measurements we have extracted a value for coefficients α and β using the pulse energies in place of the intensity. From averages and standard deviations we have α =(3 ± 1) m^{-1} and β =(20 ± 20) μJ^{-1} m^{-1}. Our estimation of coefficients is pretty much fluctuating being influenced by the systematical error in determining the coupling efficiency between core and radiation. Nevertheless the values of the two coefficients are able to reproduce the results for longer fiber within the order of magnitude.

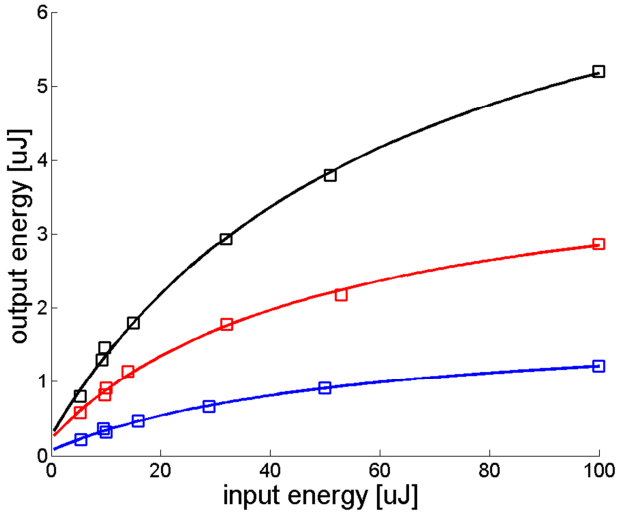

Figure 32 – Energy transmitted by the fiber at 205 nm for different fiber lengths. Black - 30 cm. Red – 70 cm. Blue – 103 cm.

At this point in our development of the optical system we tried a combined solution of two fibers, very similar to the one adopted for the infrared line. In fact we were interest in determine whether or not a fiber transport solution could be applied for AEGIS. At the end of our measurements we found out that the transmission coefficient of the line was too poor dumping the input power for 3 orders of magnitude. The direct consequence is that the system, brought at full power, would have reached the saturation fluency for the transition 1→3 of Positronium for a very narrow beam of FWHM even below 1 mm.

From the first attempts to measure the power transferred by the fiber it was possible to observe a great attenuation with respect to the incoming light. Starting from hundreds of µJ after 30 cm of fiber it was possible to measure only a few micro Joules in the exiting pulse. With this attenuation factor the output power was very poor; so tiny to be comparable to background noise due to light diffused and scattered by the other optical equipment of laser system. Moreover it was really close to lowest measurable quantities of our power meter, thus complicating measurement procedures.

In what follows we are giving a detailed description of the procedure adopted to extract 205nm energies at the entrance and in output by the fiber. The power meter is made by a thin piezoelectric slab circular in shape to be placed in front of the beam. Each pulse gets absorbed by the material causing a slight dilatation of the slab. This shape modification is converted by piezoelectric effect into a small current, signature of the energy released by the pulse into the medium. Its control circuit has current threshold value, i.e. a pulse energy threshold that should be overcome to trigger acquisitions. Otherwise vibration of the optical table could be misinterpreted as light pulses. Since minimum threshold for pulse power was a little less than 1 µJ we have been forced to add a constant background to each acquisition. As a matter of fact we have come through a few experimental situations where the energy transferred by the fiber was on edge or even below threshold, thus requiring additional power to start the acquisition. For this reason we recollect the leakage from the Brewster plate of the infrared

breadboard to add a constant bias of 1 μJ to each acquisition. Over this constant and controlled background we have been able to isolate other two background sources. They belonged to the branches of the experiment before the Sum Frequency Generation, i.e. where the production of the 205 nm takes place. The two background noise was belonging to the 894 nm and 266 nm branch. These pulses are in fact the two radiations that build up the 205 nm. As first consequence they have almost the same directionality of Positronium excitation beam. Thus it was impossible to get rid of these additional noise sources with paper shields placed around the power meter. As second drawback the modification of their intensity was the simplest and straightforward method to adjust the 205 nm power output: as consequence of any changes in their power we could register a variation of the background values. Finally their background biases were different at the entrance and at the output of the fiber. This is a direct consequence of the fact that these frequencies are less attenuated in propagating along the silica fiber core than the ultraviolet at 205 nm. Indeed it was possible to measure slight perturbation in input (10%), but much relevant modification on the opposite side of the fiber. As consequence they must be measured to be subtracted from signals. The values of backgrounds could be isolated leaving the power meter where the 205 nm is geometrically acquired and dumping alternatively one of the two branches (894 nm or 266 nm) at the beginning of the UV breadboard. In conclusion to calculate each value of 205 nm impulse power in input and output by the fiber 5 more measurement had to be taken: the trigger bias and the four additional backgrounds belonging to the pump impulses (two at the entrance and two in output).

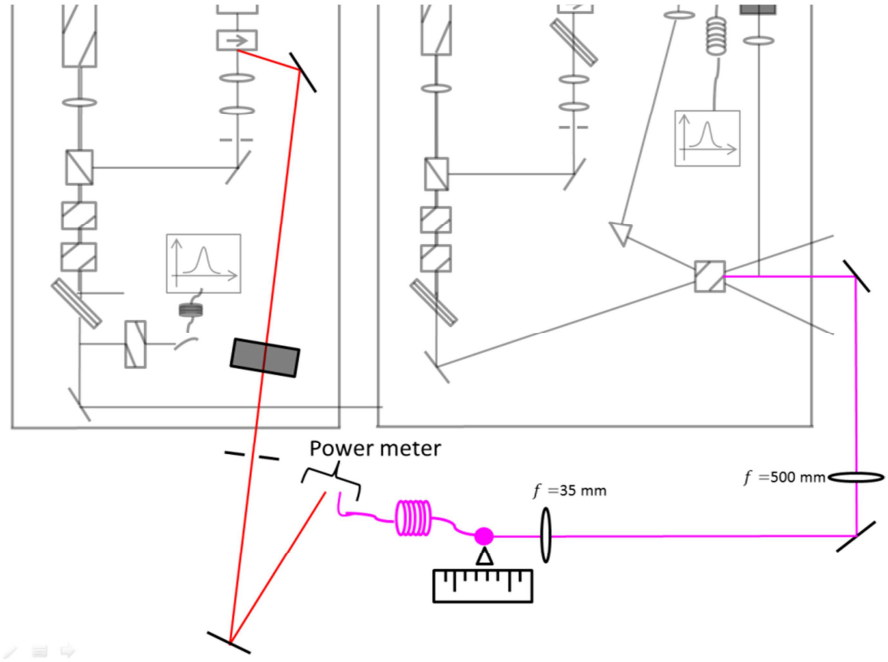

Figure 33 – Scheme of the experimental apparatus used to measure fiber transmission coefficient at 205 nm. To maximize the coupling between beam and fiber the head of the fiber was mounted on a three axis translator. The trigger background was collected from the leakage of the Brewster plate of the pump branch of the infrared breadboard, then attenuated and spatially filtered to enhance signal stability.

The energy transmission measurement had been executed using short group of pulses (20-100). In this regime we can neglect the degradation with respect to time and pulse. To facilitate alignment procedures the fiber coupling face was mounted in the focal plane of the second lens (see Figure 33). There the beam spot have been measured to be of the same size of the fiber core as specified below. This scheme ensures us that the best coupling condition could be reached only in the focal plane due geometrical reason. In this way a precise measurement of the beam spot in that region allowed us to reconstruct the geometrical coupling factor between light and fiber.

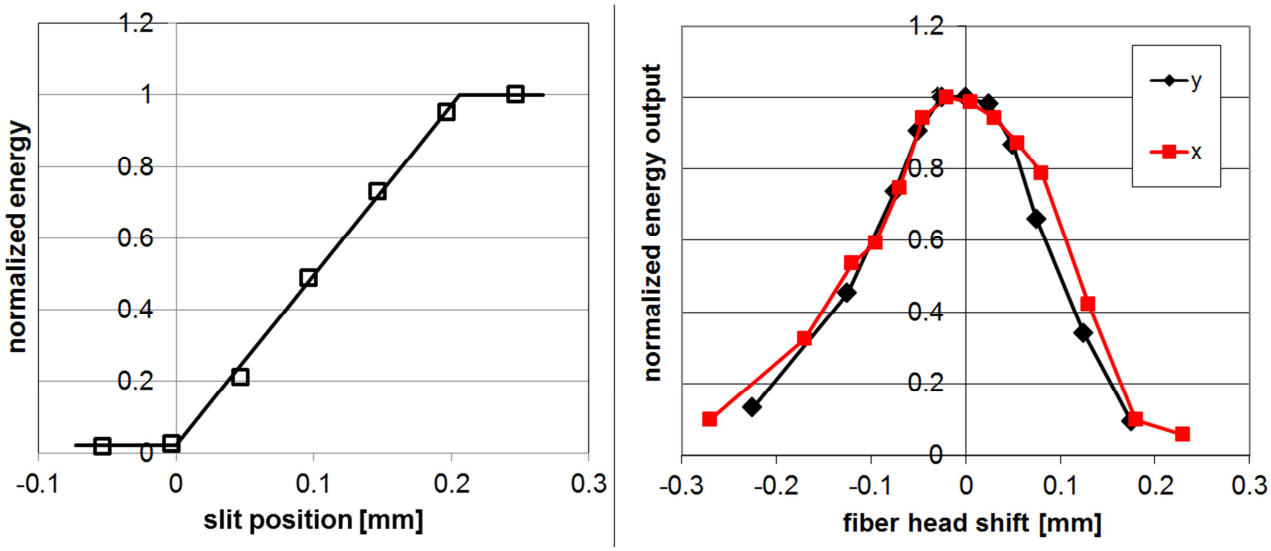

Figure 34 – Measurement of the light spot coupled with the fiber to simulate AEGIS experimental conditions. Plot to the left shows the slit measurement performed to establish the beam spot characteristics. Right plot shows the convolution profile of the beam with the circular transmitting core of the fiber. In this acquisition fiber head was moved from maximum condition (0 mm) in the horizontal (x) and vertical (y) direction.

Beam profile was investigated with a movable slit in the desired focal plane. The slit could be inserted along the beam line with sub-millimeter precision, so that the light pulse could be fully released or totally occluded. After the slit a power meter was mounted to collect residual energy for each pulse. We expected to find the minimum spot dimensions where telescopic system was reproducing the square image of the BBO crystal used for the 205 nm generation. In fact when reached this minimum the data acquired show a square and uniform intensity profile of the beam in the horizontal plane. To deduce the symmetry property of the spot fiber head was moved in vertical and horizontal direction. First we mounted the fiber looking forward maximum transfer efficiency regulating the 3-axial translator. Then, starting from the maximum we moved the fiber head in the horizontal and vertical direction alternatively. In this way we allowed the spot to be off-axis with respect to the core symmetry, thus coupling only a part of the beam. So we obtained two experimental convolution of the spot intensity profile with the circular aperture identified by fiber core region. These two curves are in good agreement one the other, thus leading to the conclusions that beam profile could be approximated by a square and uniform distribution. Then, since the square side was equal to

core's diameter, the geometrical coupling factor was calculated to be close to $\pi/4$. Experimental curves used to estimate this factor are reported in Figure 34.

We started testing the performance of the two fibers system to check suitability for AEGIS experiment. Measurement for transmitted powers follows the experimental scheme descripted above. Results are shown results in Figure 35. Since transmission coefficient was too low for AEGIS requirements we moved to a different solution with the beam transferred in free propagation.

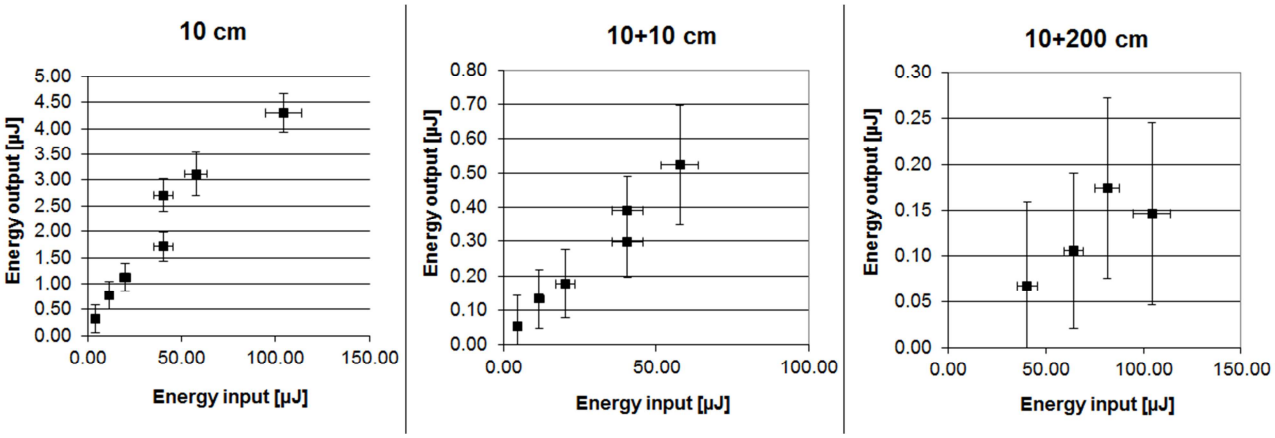

Figure 35 – Energy transmitted at 205 nm in various fiber configurations. From left to right: single fiber of 10 cm, two connected fibers of 10 cm each and two connected fibers, the first of 10 cm followed by a second of 200 cm. The latter configuration is the closest situation that could have been adopted for AEGIS.

Ultraviolet transfer line

Finally, a UV transfer line based on free propagation and traditional optical elements seem the better way to fulfill AEGIS requirements. We now describe the project and realization of this new element.

Light impulses in ultraviolet range are not transmitted by common glass and other material should be adopted to build common optical equipment. For this reason in AEGIS many lenses and prisms are made by fused silica. Transmission range of this glass allows the usage of this material not only for the excitation from ground to third levels, but also for the radiation of second transition to Rydberg Positronium.

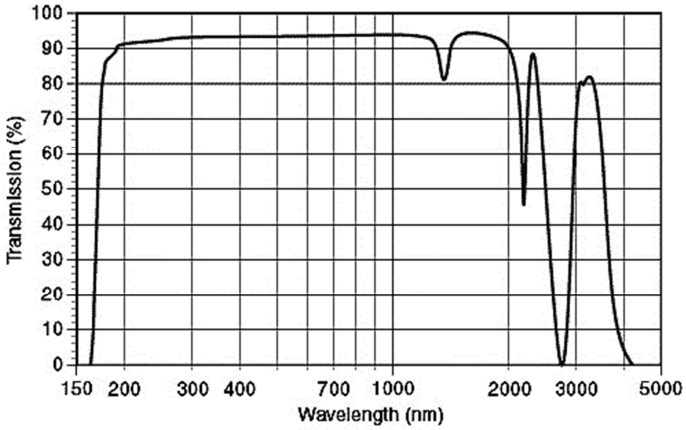

Figure 36 - UV fused silica transmission curve with respect to wavelength

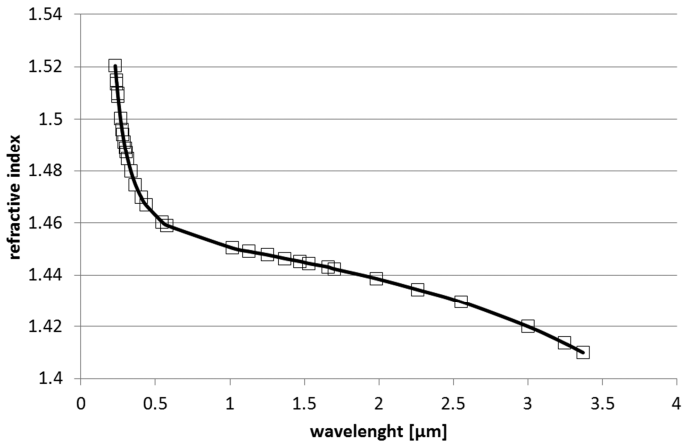

Figure 37 – UV fused silica refractive index at 26 °C with respect to wavelength

Fused silica (fused quarz) is glass consisting of high-purity silica in amorphous (non-crystalline) form. It is different from traditional glasses in which no other ingredients are added to lower the melt temperature. Fused silica, therefore, has much higher working and melting temperatures than soda-lime or borosilicate glasses. It is manufactured melting naturally occurring quartz crystals of high purity at approximately 2000 °C. The optical and thermal properties of fused quartz are superior to those of other types of glass due to its purity and as consequence it is used to make lenses and other optics for the ultraviolet spectrum. Its low coefficient of thermal expansion also makes fused silica a useful material for precision

mirror substrates. Furthermore the molecules of the material are strongly bound to each other and this glass is not degasing even in ultra-high vacuum environments. These are all good reasons to adopt this material to transfer the ultraviolet pulse inside AEGIS experiment, near the target region. As consequence the optical equipment of the transfer line are all made in fused quarz.

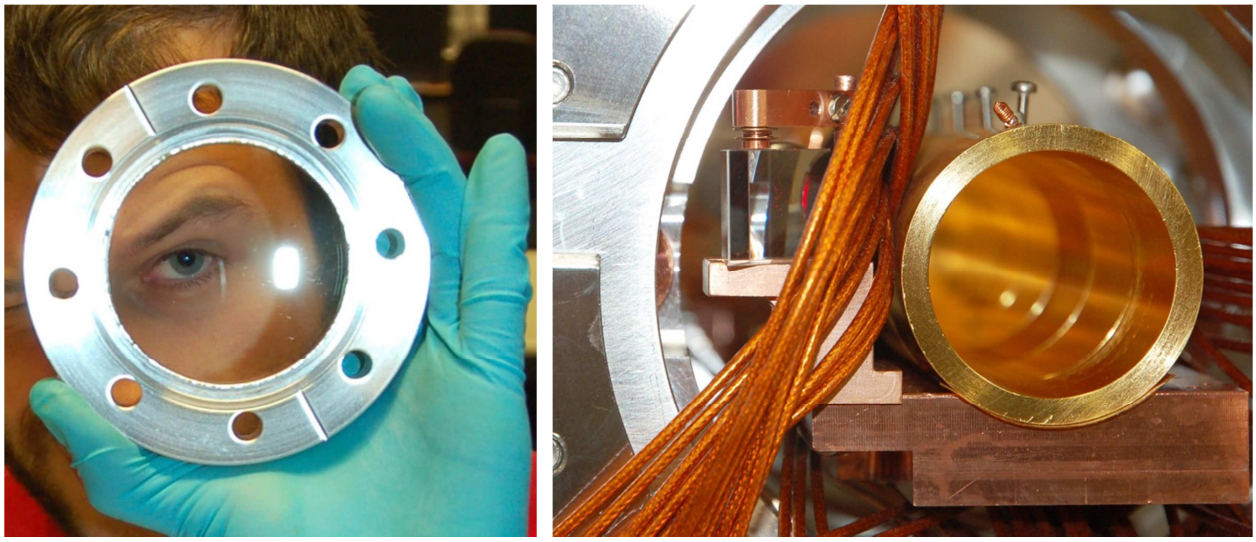

Figure 38 – On the left is visible one of the two identical viewports produced by Allectra type 63CF. On the right a picture of the first prism (2 cm side) near the trap at the entrance of the 1T magnet region.

To guide radiation in the Positronium region we adopted three prims used in total reflection. The three right angle prisms are mounted to bring light on the Ps cloud and guide it back outside. The first two prisms get light into the central region to hit the Positronium cloud, while the third reflects pulses back on their path. In order for the beam to easily complete the back path the first prism is twice bigger (2 cm side) than the other two (1 cm side). The prisms line and supports are custom made. Supports for the three prisms were designed by L.Dassa under our specification and they had been manufactured in Milano by INFN workshop.

The advantages of installing a third reflecting prism are: a reduction of the power loss dispersion in cryogenic region than the fiber apparatus and a double illumination effect of the pulse on the Ps cloud. However the main reason to require the last prism is for alignment purpose. To control the position of the beam near the silicon target it is possible to select the correct optical path using a laser diode, looking at back reflected light from the inner part of the apparatus. Directionality and coherence of the light emitted by the diode are key features in the alignment procedure. From outside we are able to make a clear identification of the actually reflected area of the third prism. Even the corner edge has turned out to be very useful, thanks to the characteristic diffraction patter caused by the linear discontinuity in the reflectance.

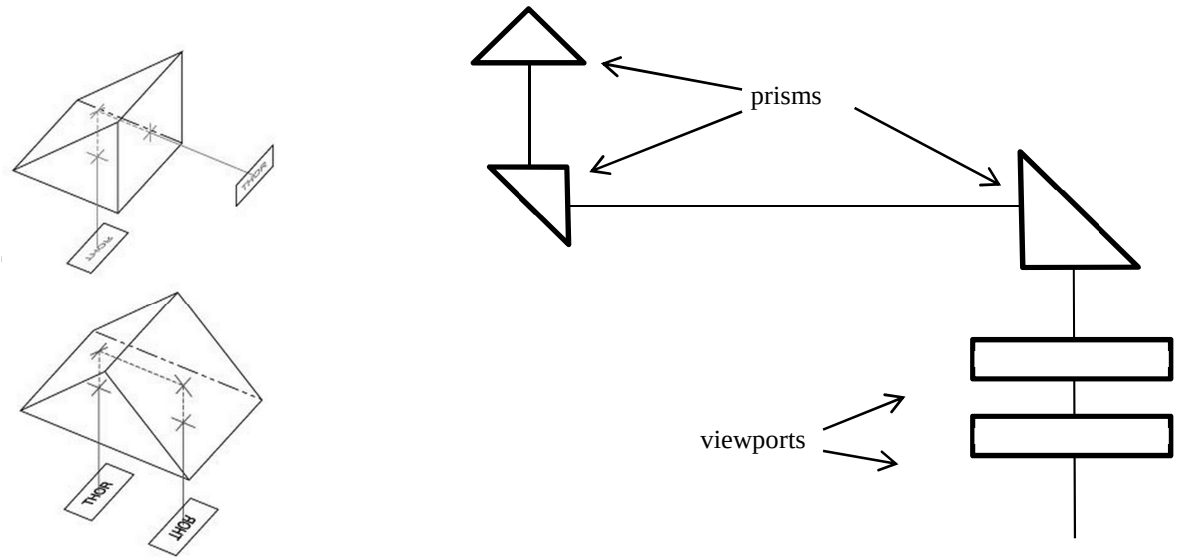

Figure 39 – Scheme of the AEGIS inner part of the ultraviolet optical system to reach the Positronium cloud. On the left is shown a representation of prisms used in total reflection to modify the direction of the beam.

With current set up alignment of the optical system can be realized in a few minutes. First, the diode laser is inserted on ultraviolet beam line. Than modifying the optical path it is look forward the reflection from last prism. Among the secondary reflections the interesting one is recognizable thanks to the diffraction pattern of the prism edge. Second step is to perform fine adjustment of beam direction looking at the shape of reflected image, i.e. directing the beam on the preferred position with respect to Si target. As a matter of fact target position can be easily identified and so this operation can be very precise. Using laser diode it is possible to achieve a pointing precision in the target region of one tenth of millimeter. Then two irises are placed at almost 45 cm one to the other on the optical table, outside the viewports. They should indicate the correct direction that is selected by diode radiation. At this point alignment laser can be removed and ultraviolet pulses can be directed along the same path with the help of the irises. This procedure has shown to obtain an overall precision of 0.5 mm in the target region. This result could be considered satisfactory since the beam size in that region should be between 3 to 8 mm in diameter.

Almost the totality of this optical path is carried on in vacuum with a light propagation speed much higher than for the fiber transport line. The path from the first viewport to Positronium region is of 153 cm. However the two time of flight needs to be adjusted in order to make ultraviolet arriving in time coincidence as much as possible with the infrared pulse. To perform alignment procedure, mount irises, adjust beam size and pulse delay we added a fourth breadboard on the optical table.

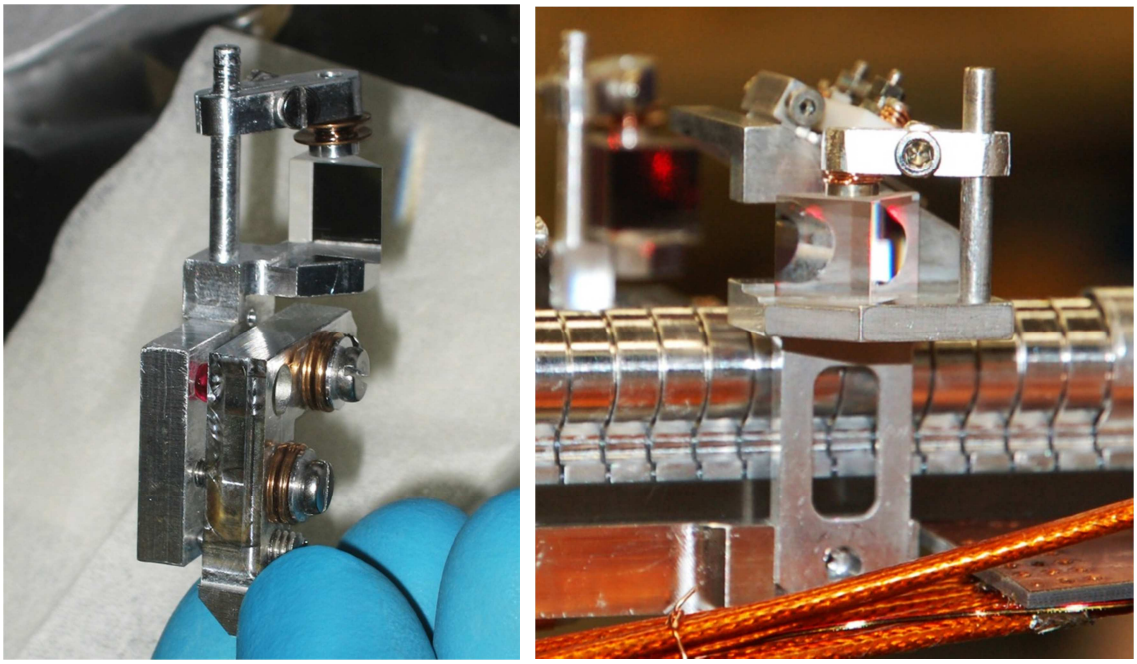

Figure 40 – Second (left) and third (right) prisms of the optical system. The holder of the second prism is adjustable over two rotation axes.

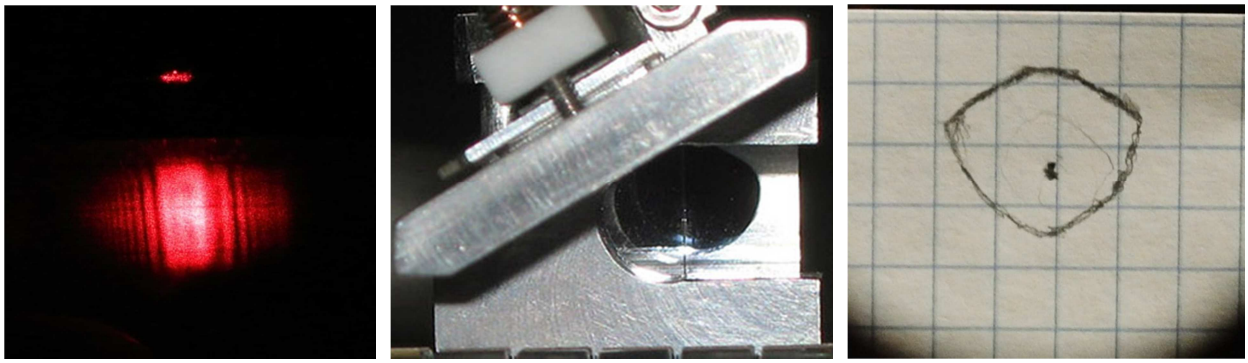

Figure 41 – From left to right. Diffraction pattern belonging to prism (over a secondary reflection). Direct picture of the reflecting region by the third prism (the height of the aluminum cut is 8 mm). Reconstruction of the reflecting region on the optical table using the alignment laser diode.

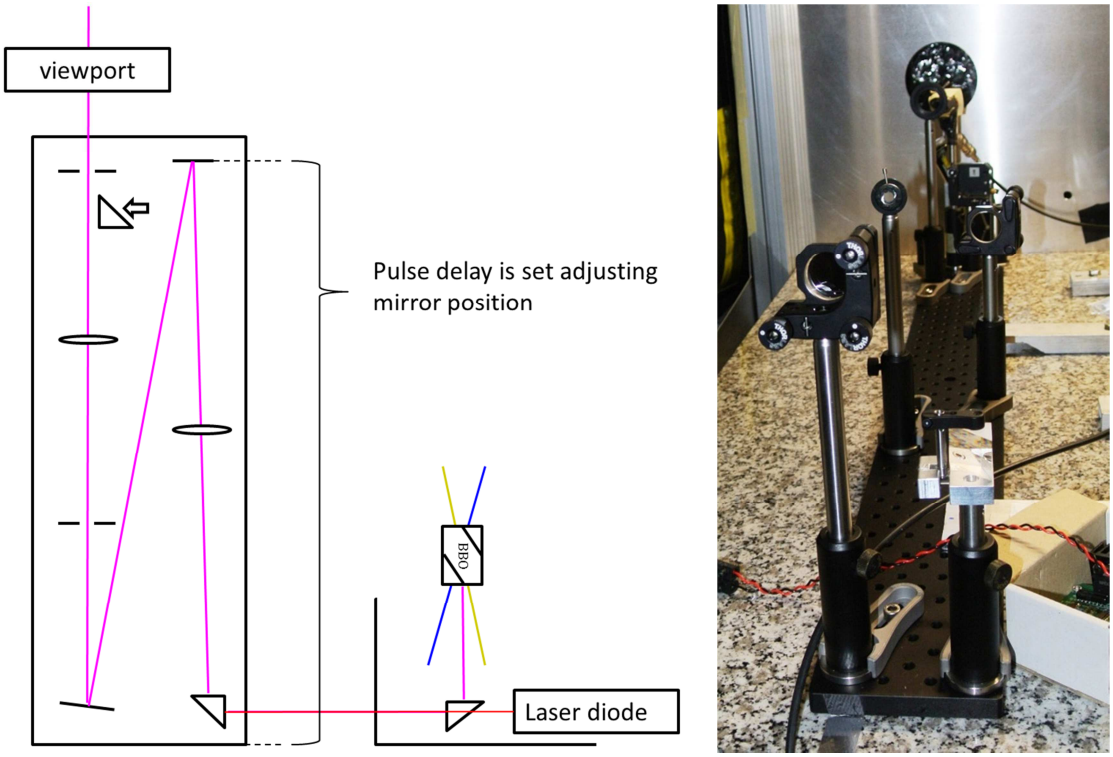

Figure 42 – Breadboard for ultraviolet pulse, drawings and picture. Breadboard size is 10x90 cm

During breadboard assembly measures have been taken of each optical element position in order to calculate the optical path length and compare it with that of the infrared radiation. To control the calculations a measurement of the delay was performed on the optical table. A photodiode was placed along the optical path first near the BBO crystal and then near the viewport. Like all the other optical elements its absolute position with respect to the breadboard was taken. In this way it was possible to perform both the time of flight measurement and the calculation. Furthermore measurements of the achievable delays have been performed adjusting the position of one reflecting mirror as suggested in Figure 42. Results of this experiment are reported in Figure 43. To correctly perform synchronization between ultraviolet and infrared radiation we measured the mutual delay of 205 nm after BBO and 1650 nm at fiber coupling finding 0.9 ns.

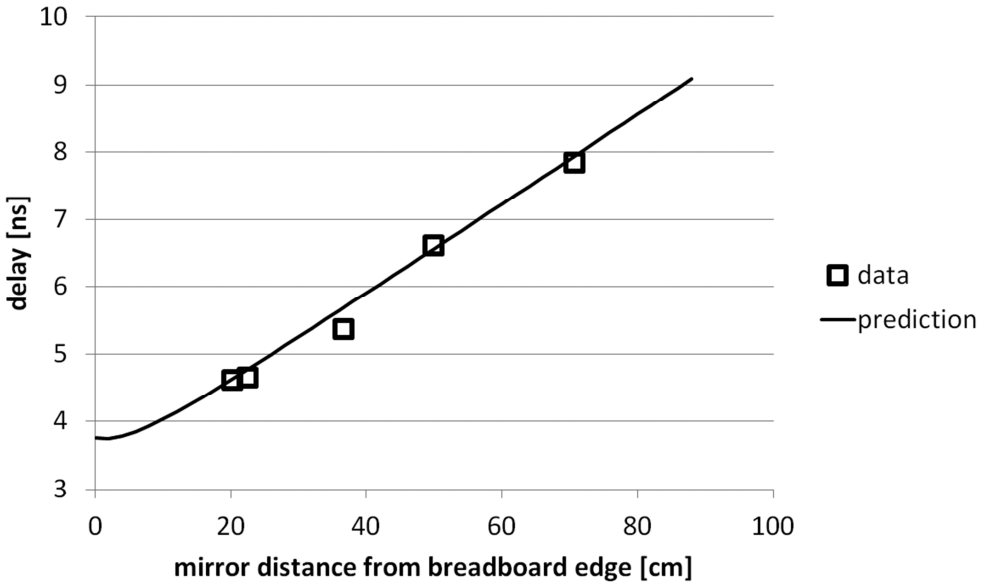

Figure 43 – Measured performance of the delay line for the ultraviolet pulse. The delay is set moving the first reflecting mirror. As indicated in Figure 42 position of the mirror for each acquisition was measured from the edge of the breadboard. The prediction curve is calculated and shown in the plot with a continuous line.

At each interface between vacuum and fused silica pulses lose a little fraction of their power because partial reflection induced by discontinuity in the refractive index. Knowing the refractive index of fused silica at 205 nm ($n \approx 1.54$) the transmission coefficient T of the single interface can be easily calculated by the well-known formula

$$T = \frac{4n}{(1+n)^2} \approx 95.5\%$$

As consequence total transmission coefficient of a viewport or a prism is almost T^2 =91%. Hence total transmission coefficient should be calculated multiplying all contributions coming from the optical elements mounted between generation crystal and Positronium. Each element introduces a little loss, so to calculate an equivalent transmission coefficient for the entire optical path all contributions have to be propagated over the transfer line. Accounting that mirrors have a reflecting coefficient R =95% the total transmission coefficient should be

$$T_{tot} = T^{16}R^2 \approx 43\%$$

This can appear a very poor result, but is definitely huge compared to the transmission coefficient achievable with fibers that was close to 0.1% . Moreover the reflectance from the third prim is doubling the effect of the pulse thus restoring the bigger amount of lost power. Reflecting effect can be accounted with a modified transmission coefficient of

$$T^*_{tot} = T_{tot}(1+T^2) = 82\%$$

Conclusions

Now it is worth concluding this report calculating parameters of the optical system in an experimental like situation that could happen during AEGIS runs. Starting from a few assumptions we will be able to calculate the optimal working condition for laser apparatus and optical system. Certainly many of the parameters we are now assuming or deducing will require adjustment and regulations during realization of the experiment. Nevertheless it is possible to predict a typical working condition starting from topics described along the text.

At first we need that the UV and IR pulses arrive on Positronium cloud in coincidence for the search of the maximum efficiency in excitation. We are interested in not interleaving a great time between arrivals of the pulses, because Positronium could spread out pretty fast from target surface. Now, since infrared fiber is at the moment 250 cm long, we deduce from Figure 44 that the ultraviolet mirror could be placed at 20 cm from breadboard edge to synchronize pulses.

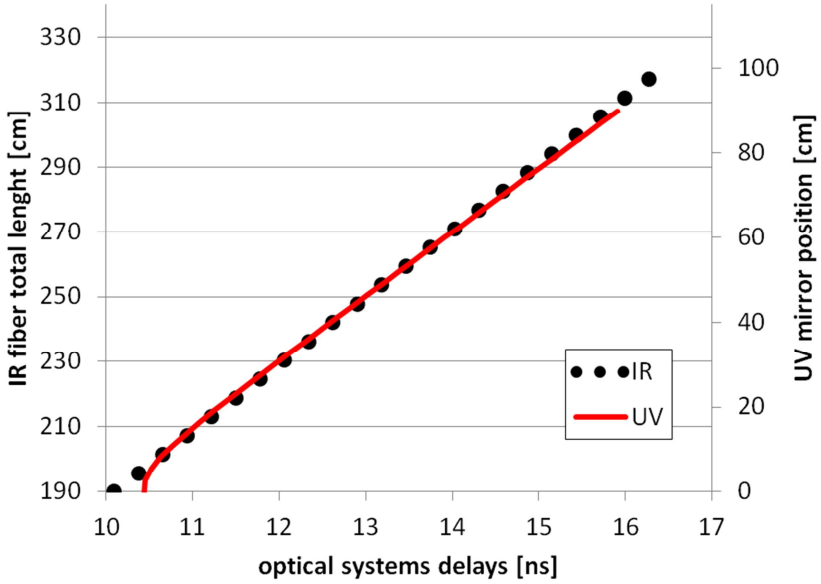

Figure 44 – Comparison of the delays of the optical system to be used for estimating UV mirror position with respect to breadboard edge

So the lightning time of the Positronium cloud will be the duration time of the radiation pulse that should be of 5 ns. Unfortunately using time of flights of Ps only, combined with the 5 ns of light duration only we cannot estimate the required dimensions of laser beam, because positrons implantation could jitter with respect to pulses of about 5 ns. For this reason it would be better to anticipate the positrons shot of about the same amount. At this point it is straightforward that the beam spot must be as large as the cross dimensions of the Positronium cloud at 10 ns or more after implantation. In this way we ensure that the whole cloud gets illuminated by both pulses. The fast branch of the curve adopted to fit Positronium cloud is contained within a hemisphere that is linearly increasing in time as shown in Figure 45. Using the plot and assuming our Ps temperature fit of 1000-1500 K we obtain the beam spot diameter: 5-6mm. It would be better to adopt a 6 mm dimensions due to the 0.5 mm

uncertainty in alignment procedure. Final step is to determine minimum required energies for ultraviolet and infrared pulses. Using saturation fluency values we obtain respectively: 40 and 280 µJ on Positronium and 50 µJ and 1.1 mJ before the entrance of the optical system.

Finally we suggest the adoption of a longer fiber bringing the total length of the fiber path to 270-290 cm. This could be helpful during the assembly operation of the experiment.

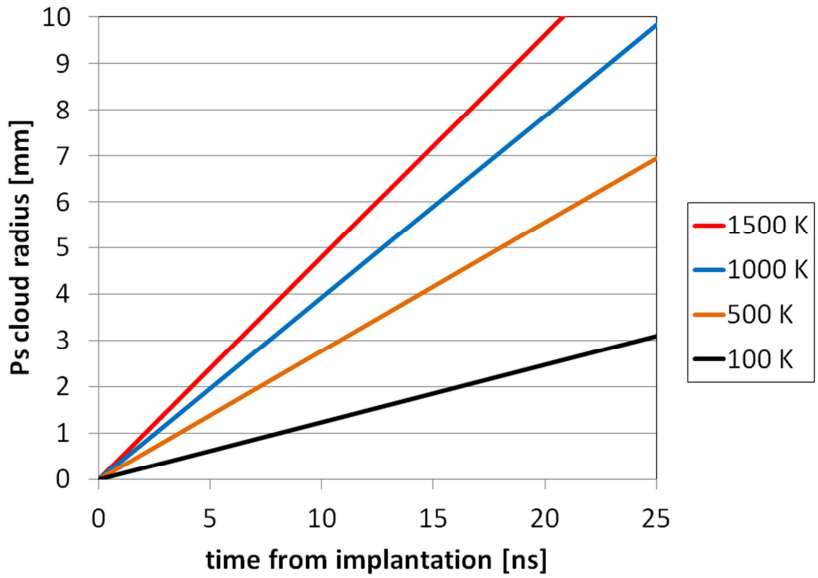

Figure 45 – Time dependence of the Positronium cloud radius with respect to time and different temperature distributions

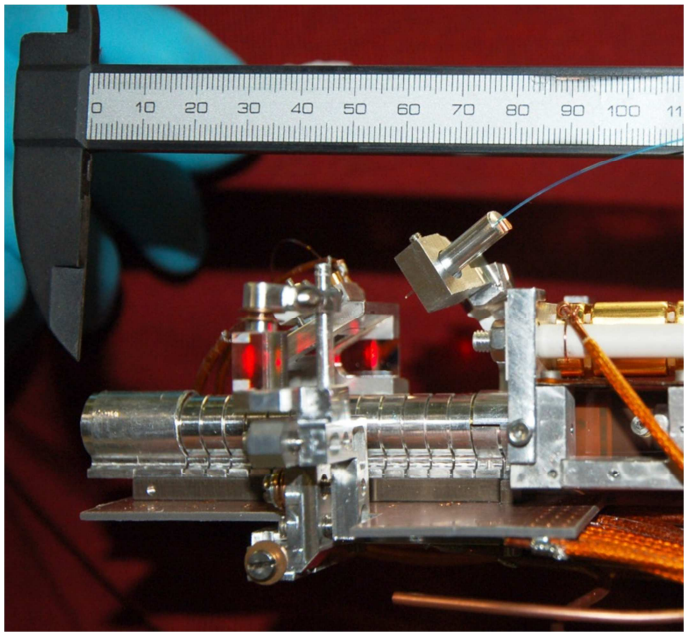

Figure 46 – In picture is shown the excitation region of Positronium over the antiprotons trap. In picture are visible most of the components of the optical system developed during the thesis work.

Future developments

The Antiproton Decelerator is now closed and a further improvement, the ELENA deceleration ring, will be assembled during the next two years. ELENA is a compact circular decelerator for cooling further 5 MeV antiprotons delivered by AD. As mentioned in AEGIS set-up, most of antiprotons produced are lost due to the use of degrader foils needed to decelerate them from the AD injection energy down to around 5 keV; an energy suitable for trapping. By using a ring equipped with beam cooling, high deceleration efficiency and an important increase in phase-space density can be obtained, resulting in an increased number of trapped antiprotons. Decelerating to these low energies is new and will be very challenging both in designs of the different elements and for ring operation.

In meantime AEGIS will continue to prepare the apparatus and the experimental procedures to perform the gravity measurement.

The technique of Positronium production and excitation will be investigated in a different and controlled environment. A dedicated apparatus has been prepared for the explicit study of the excitation process and the energy levels of Positronium. This experiment will pave the way for antihydrogen synthesis, preparing procedures and expectations values for the distribution levels of the excited Positronium. So during the next month the laser apparatus is foreseen to be put into operation. There the optical breadboard here realized to prepare and synchronize the ultraviolet pulse will be adopted with only slight modification.

The other components of the developed optical system in the inner part of AEGIS are foreseen to be used in the near future. An injector of protons is in fact under realization to provide nuclei to the experiment. Since Positronium is a symmetric atom then the technique for antihydrogen synthesis could be adopted to prepare hydrogen atoms. Thus the whole apparatus could in principle be tested with ordinary matter, realizing a reference gravity measurement to be confronted with antimatter behavior.

Appendix

Laser maintenance

To preserve full performances of the laser apparatus a few maintenance operation should be carried on from time to time. The most important are reported in EKSPLA manual and concerns the specific maintenance of the laser cavity such as cleaning of the optics or substitution of the laser flash lamp (every 6 months). In addition to this we have noticed a degradation of the BBO crystal dedicated to the SFG of the 205 nm due to the high intensity of the ultraviolet beam at 266 nm used in the generation process. We thus recommend to periodically (every 3 month) check of the crystal, the beam shape and the power output in order to substitute the crystal if needed.

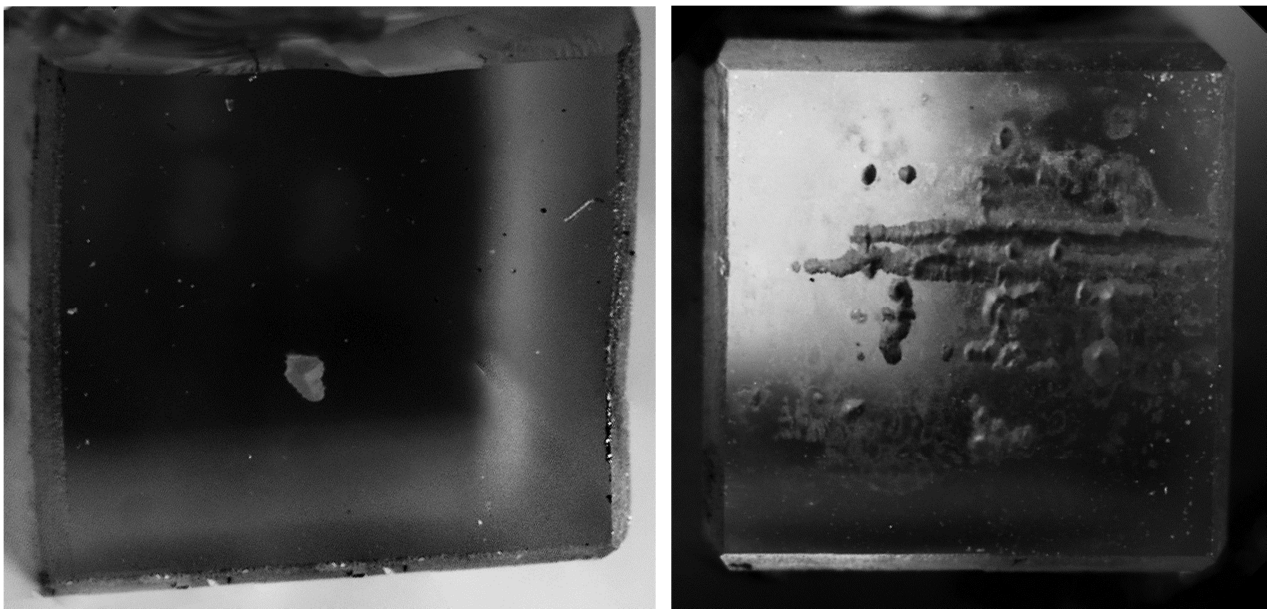

Figure 47 – Microscope image of the front face of the BBO crystal used for the SFG of 205 nm. Side of crystals are 4mm in lenght. On the left one almost new crystal and on the right the crystal used for 6 month to test the laser system in Milano

Bibliography

[1] J.F. Donoghue, Phys. Rev. D 50 (1994) 3874, doi:10.1103/ PhysRevD.50.3874.

[2] P. Morrison, Am. J. Phys. 26 (1958) 358, doi:10.1119/1.1996159.

[3] L.I. Schiff, Phys. Rev. Lett. 1 (1958) 254, doi:10.1103/ PhysRevLett.1.254

[4] M.C. Fujiwara et al., *Three-Dimensional Annihilation Imaging of Trapped Antiprotons*, Phys. Rev. Lett. Vol.92 n.6 (2004)

[5] C.H. Storry et al., *First Laser-Controlled Antihydrogen Production*, Phys. Rev. Lett. 93, 263401 (2004)

[6] A. Kellerbauer and J.Walz, *A novel cooling scheme for antiprotons*, New Journal of Physics 8 (2006) 45

[7] M.H.Holzscheiter et al., *Antihydrogen production and precision experiments*, Nuclear Physics B (Proc.Suppl.) 56A (1997) 336-348.

[8] A.Kellerbauer et al., *Proposed antimatter gravity measurement with an antihydrogen beam*,Nuclear Instruments and Methods in Physics Research B 266 (2008) 351–356

[9] M.K. Oberthaler et al., *Inertial sensing with classical atomic beams*, Phys. Rev. A 54, 3165 (1996)

[10] M. Charlton and J.W. Humberston, Positron Physics, Cambridge University Press, chapter 6 (2000)

[11] R.J. Hughes, M.H. Holzscheiter, Phys. Rev. Lett. 66 (1991) 854.

[12] E.S.Chang, *Radiative lifetime of hydrogenic and quasihydrogenic atoms*, Phys. Rev. A vol. 31, n.1

[13] S.Mariazzi, A.Salemi, R.S.Brusa, *Positronium cooling into nanopores and nano channels by phonon scattering*, Phys. Rev. B 78, 085428 (2008)

[14] S.Mariazzi, P.Bettotti, S.Larcheri, L.Toniutti, R.S.Brusa, *High Positronium yield and emission into the vacuum from oxidized tunable nanochannels in silicon*, Phys. Rev. B 81, 235418 (2010)

[15] S.Mariazzi, P.Bettotti, R.S.Brusa, *Positronium Cooling and Emission in Vacuum from Nanochannels at Cryogenic Temperature*, Phys. Rev. Lett. 104, 243401 (2010)

[16] F.Castelli, I.Boscolo, S.Cialdi, M.Giammarchi, *Efficient Positronium laser excitation for antihydrogen production in a magnetic field*, Phys. Rev. A 78 052512 (2008)

[17] S. Cialdi, I. Boscolo, F. Castelli, F. Villa, G. Ferrari, M.G. Giammarchi, *Efficient two-step Positronium laser excitation to Rydberg levels*, Nuclear Instruments and Methods in Physics Research B 269 (2011) 1527–1533

[18] F.Ferri, *PROGETTAZIONE E REALIZZAZIONE DI UN SISTEMA LASER PER L'ECCITAZIONE EFFICIENTE DEL POSITRONIO A LIVELLI RYDBERG*, master thesis, supervisior: S.Cialdi, co-supervisor: F.Castelli

[19] F.Villa , *Laser system for Positronium excitation to Rydberg levels for Aegis experiment*, master thesis, supervisior: S.Cialdi, co-supervisor: F.Castelli

[20] D.B.Cassidy, T.H.Hisakado, H.W.K. Tom, A.P.Mills, *Efficient Production of Rydberg Positronium*, Phys. Rev. Lett 108, 043401 (2012)

[21] P.Karlitschek, G.Hillrichs, K-F.Klein, *Photodegradation and nonlinear effects in optical fibers induced by pulsed uv-laser radiation, Optics Comunication*, 116 (1995), 219-230

[22] R.K.Brimacombe, R.S. Taylor and K.E.Leopold, Dependence of the nonlinear transmission of fused silica fibers on excimer laser wavelenght, J. Appl. Phys. 66 (1989) 4035

[23] Yariv A., Yeh P., *Optical Waves in Crystals Propagation and Control of Laser Radiation*, Wiley Series in Pure and Applied Optics 1984

[24] O.Svelto, D.C.Hanna, Principles of Lasers, 5th edition, Springer 2010

[25] Geoffrey New, *Introduction to Nonlinear Optics*, Cambridge University Press, 2011

[26] J.D.Jackson, *Classical Electrodynamics*, 3rd edition, Hamilton Printing Company, 1999

[27] J.H.Wray, J.T.Neu, *Refractive Index of Several Glasses as a function of Wavelenght and Temperature*, J. Opt. Soc. Am. Vol. 59 n.6

[28] www.rp-photonics.com

[29] www.thorlabs.com

[30] www.allectra.com

[31] aegis.web.cern.ch/aegis/Proposal/Proposition.pdf

Acknowledgments

I want to acknowledge Marco Giammarchi for his support during the thesis period both at Milano and at CERN and Daniele Cipriani for his help in technical works in laboratory. I want to acknowledge INFN for the economic support during the permanence periods at CERN and for the manufacturing of the pieces of the optical system installed in AEGIS.

A special acknowledge goes to Ruggero, who worked on the laser system for his master thesis and with whom I shared good working day, but above all wonderful holydays.

Further I would like to add a few acknowledgments of secondary importance to people who helped me, or shared with me days and experiences, but even a few circumstances that entertained me during this year. First Miri, my favorite engineer. Marta e Ugo for their willingness in helping me in everyday life. AEGIS people: the first lady, the cabling team, people that are looking for founding or for mercy, students that were at CERN by chance and the person needing for a purpose to be at CERN. Parsley, for all the troubles that we caused each other. The “simpatico” child, and the nuclear misadventure caused by scientists. Luca for is patience. Trains that does not exist, but which are still able to bring people in Geneva. E-mails that cannot be read with a special accent. The canceled order, because phone loud speaker had extended the enthusiasm to everyone in AEGIS control room. The “fischiatina” jingles. Frequented Evo meeting. “Chiacchiere” and ice cream, wonderful sweets during the carnival or summer. EKSLPA for providing us a reliable system, the big red button to be pushed in case of success and the fried chicken. Holzer, that have remind me how things that appear impossible could be realized.

Finally I wish that menisci and valves would keep people who worked with me in good health.